Highly Efficient Mesoporous Mg/γ-Al2O3 Catalysts for Ozonation of Saline Petroleum Effluents

Renshun Xu, Hervé Nabet, Audrey Breton, Patrick Baldoni-Andrey, Nicolas Lesage, Thomas Cacciaguerra, Vasile Hulea, Francois Fajula, Anne Galarneau

Highly efficient mesoporous Mg/γ-Al_2O_3 catalysts for ozonation of saline petroleum effluents

Renshun Xu,[a] Hervé Nabet,[b] Audrey Breton,[b] Patrick Baldoni-Andrey,[b] Nicolas Lesage,[b] Thomas Cacciaguerra,[a] Vasile Hulea,[a] Francois Fajula,[a] Anne Galarneau [a*]

[a] Institut Charles Gerhardt Montpellier - Univ Montpellier- CNRS - ENSCM, 240 avenue du Professeur Emile Jeanbrau, Montpellier, France.

[b] TOTAL SA, Pole d'Etudes et de Recherche de Lacq, Lacq, France.

**e-mail: anne.galarneau@enscm.fr*

Abstract

γ-Al_2O_3 is promising for catalytic ozonation because it produces HO° radicals. To improve its basicity and/or its oxidative character, highly mesoporous γ-Al_2O_3 was doped with different metals M alone or in mixture (M = Mg, Ca, Zn, Fe, Ba, Zr, Cu, Co, Ni, Ce, Ti, with 0.05 < M/Al < 0.5 molar ratio) prepared either by incipient wetness deposition or by direct sol-gel. Tests to determine the basic and oxidative character of the catalysts have been set up. Results show that Mg-doped alumina materials exhibited the highest basicity and Cu,Mg-doped alumina materials the highest oxidative character. These materials (5 g/L) were tested in the catalytic ozonation of a synthetic saline (NaCl = 50 g/L) petroleum effluent such as produced water (TOC = 216 mg/L) containing phenols, acetic acid and polycyclic aromatic hydrocarbons. Among these catalysts, Mg-doped alumina with molar ratio Mg/Al = 0.1, 0.2 prepared by incipient wetness deposition were the more efficient catalysts. Under reuse the Mg-doped alumina catalyst (Mg/Al = 0.1) exhibited the highest ozonation rate with 98% TOC removal in 5 h. This remarkable behavior was attributed to the *in-situ* formation during ozonation of spinel ($MgAl_2O_4$) nanoparticles at the surface of Mg-doped alumina particles.

Keywords: Catalytic ozonation; Water treatment; Saline effluents, Alumina, Basicity; Oxidation.

INTRODUCTION

Catalytic ozonation is expected to become a central technology for the processing of contaminated aqueous effluents containing non-biodegradable toxic organic residues (For a recent review see *eg* [1]). Compared to established methods, such as adsorption, coagulation, flocculation, incineration, membrane separation or biological oxidation, catalytic oxidation should allow higher degradation efficiency with lower energy consumption, lower footprint and, accordingly, lower operation and investment costs.

Catalytic ozonation, as part of advanced oxidation processes, can be operated at ambient temperature and pressure with total mineralization of the organic substrate into carbon dioxide and water. This is a significant advantage compared to single ozonation of organic matter, which usually leads ultimately to the formation of aldehydes and carboxylic acids, which do not react with ozone. Though the mechanism of the reaction is not fully resolved and subject to debate [2], the role of the ozonation catalyst is, schematically speaking, to promote, on the one hand, the formation of hydroxyl radicals, able to degrade all types of organics and intermediates by ozone decomposition and, on the other hand, the adsorption of ozone and the organics present in the effluent, both effects contributing to enhanced kinetics.

Regardless the catalytic system under consideration, homogeneous or heterogeneous, catalytic ozonation reveals very complex and the chemical pathways involved depend on many factors such as the experimental conditions, the nature of the substrate and of the intermediate oxidation by-products, the chemical nature, the texture, the stability and the amount of catalyst. With respect to heterogeneous catalytic ozonation, supported metals (Cu, Pt, Ce, Ru, Mn,…), metal oxides (MnO_2, MgO, TiO_2, Al_2O_3, CeO_2, …), modified zeolites (MFI, LTA, FAU) and mesostructures (SBA-X, CMK, M41S), activated carbons and combinations of the above have been reported [1,2]. Raw minerals such as perovskites, bauxite and goetite have been used also in catalytic ozonation [3-5]. As a common requirement for these materials to be active is the necessity to adsorb ozone and organic matter at their surface. Though gas phase adsorption of ozone and organics is well described, adsorption of ozone on polar or apolar surfaces in the presence of an excess of water is far from being documented and clearly understood. For this reason, several mechanisms and catalytic active sites have been suggested to account for the activity of solid surfaces to decompose ozone such as (i) oxidized or reduced forms of supported metals [6], (ii) Lewis centers of metal oxides [7], (iii) non-dissociated hydroxyl groups of metal oxides [8-10] and (iv) basic centers of the catalyst surface [11-13].

In a precedent study [13] we have investigated the catalytic ozonation of 2,4-dimethyl phenol (2,4-DMP) and of a model petrochemical effluent containing a mixture of phenol, acetic and

naphtenic acids, pyrene, and naphtalene using various catalytic materials featuring an acidic (zeolites, mesoporous alumino-silicates), basic (ion-exchanged zeolites), amphoteric (γ-alumina), oxidative (titanium oxide) or neutral (silica) surfaces. Among them, γ-alumina proved the most efficient.

Conflicting conclusions are reported in literature regarding the activity of γ-alumina for ozonation. For instance, the ability of γ-alumina to generate free radicals by interaction of ozone with hydroxyl groups is put forward in several papers [6,8,13-18], but the chemical nature of the catalytic active sites is subject of debate. Neutral OH groups [17,19] or Brönsted acidic sites [20] have been proposed. This hypothesis is supported by the fact that nitrates or sulfates inhibit the activity of the surface by substitution of reactive hydroxyls. On the contrary, Oyama *et al.* [21] reported no activity for mere alumina surfaces and suggested that it could play a single role of support for metal or metal oxides with Lewis acidity or oxidative properties. As an alternative hypothesis, the generation of hydroxyl radicals has been attributed to reaction of ozone with adsorbed molecules [18,22]. In that case, ozonation activity would be controlled by the adsorption of the organic substrates and intermediate oxidation products on the surface of γ-alumina rather than by the presence of reactive hydroxyl groups.

The difficulty in clarifying the catalytic role of alumina surface in the ozonation reaction stands in the fact that, not only the surface may undergo chemical and structural modification during the reaction, but also, as said above, the process is highly dependent on the operation conditions. Among others, the conditions of the activation of the catalyst, the nature of the substrate and the pH of the medium have a dramatic impact on activity. For instance, non-polar substrates such as aromatic hydrocarbons [23] and ethers [24] do not adsorb and react in the presence of alumina under conditions where ozone is readily decomposed and able to oxidize fulvic and humic acids, which showed a high affinity for the alumina surface [18]. The influence of pH is complex as it can affect the overall process. Thus, depending on pH value, hydroxyl radicals can be consumed by condensation to generate hydrogen peroxide [15] and strong adsorption of intermediate carboxylates may occur for pH values lower than the pH_{zpc} resulting in lower activity and low stability of the catalyst.

By combining ozonation experiments with surface characterization by infra-red spectroscopy and gravimetric sorption measurements, we have proposed that the activity of γ-alumina results essentially from the basic character of its hydroxylated surface and to its high capacity in adsorbing carboxylic acids [13]. The use of tert-butanol as radical scavenger suggested the involvement of hydroxyl radicals in the reaction [13]. The addition of NaCl neutralized 70%

of HO° during the catalytic ozonation of 2,4-dimethyl phenol (2,4-DMP) as chloride ions present a very strong scavenging effect on radicals [13]. However the addition of NaCl to the aqueous effluent containing polycyclic aromatic hydrocarbons (PAHs), phenol and acetic acid allowed to increases the total organic carbon removal from 50% to 90%. The results suggest that sodium cations prevent carboxylic acids adsorption on the basic sites of γ-alumina whereas chloride anions give Cl_2 or chlorine radicals prone to oxidize PAHs, which in turn produce HO° by intermediate in-situ formation of H_2O_2 [13]. The latter is then able to react with acetic acid to form peracetic acid, a very powerful oxidant.

In order to deepen our understanding of the catalytic role of γ-alumina in the ozonation reaction we have undertaken a systematic study of the modification of its surface using a series of metal promoters or modifiers (Mg, Ca, Zn, Fe, Ba, Zr, Cu, Co, Ni, Ce, Ti) either by incipient wetness deposition or by direct sol-gel (sg) synthesis. These metals have been selected in order to improve the basicity and/or the oxidative character of the alumina surface. Two specific tests, for measuring the basicity of the materials in water and for estimating their redox behavior have been developed. The performances of characteristic materials have been then evaluated in the ozonation of a model petrochemical effluent.

EXPERIMENTAL

Materials

Synthesis of metal-doped aluminas by incipient wetness deposition on γ-alumina

γ-Al_2O_3 (Alfa Aesar, powder obtained by grinding the original particles) was used as a support for all syntheses. In a typical incipient wetness impregnation, 2 g of γ-Al_2O_3 were mixed with 2-3 mL of aqueous metallic salt (x g) (Table 1) solutions for 24 hours. The samples were then dried for 24 h at 80 °C and calcined in air at 450, 600 or 750 °C for 5 h.

Table 1. List of metal-doped aluminas prepared by incipient wetness with 2 g γ-Al_2O_3

Catalyst	Metal salt	Metal salt g	Metal/Al molar ratio
γ-Al_2O_3	none	0	0
Mg/γ-Al_2O_3	$Mg(NO_3)_2.6H_2O$	2.0	0.2
Mg/γ-Al_2O_3	$Mg(NO_3)_2.6H_2O$	1.18	0.12
Mg/γ-Al_2O_3	$Mg(NO_3)_2.6H_2O$	0.60	0.06
Mg/γ-Al_2O_3	$Mg(NO_3)_2.6H_2O$	0.30	0.03
Mg/γ-Al_2O_3	$Mg(NO_3)_2.6H_2O$	0.15	0.015
Mg/γ-Al_2O_3	$Mg(NO_3)_2.6H_2O$	0.076	0.007
Ca/γ-Al_2O_3	$CaCl_2$	0.22	0.07
Zn/γ-Al_2O_3	$Zn(NO_3)_2.6H_2O$	0.38	0.04
Fe/γ-Al_2O_3	$(NH_4)_2Fe(SO_4)_2$	0.59	0.05

Ba/γ-Al_2O_3	$Ba(NO_3)_2$	0.42	0.05
Zr/γ-Al_2O_3	$ZrO(NO_3)_2$	0.46	0.05
Co/γ-Al_2O_3	$Co(NO_3)_2.6H_2O$	0.36	0.05
Ni/γ-Al_2O_3	Ni $(NO_3)_2$	0.36	0.05
Ce/γ-Al_2O_3	C_6H_9CeO6	0.63	0.05
Cu/γ-Al_2O_3	Cu $(NO_3)_2$. $3H_2O$	0.37	0.05
Cu/γ-Al_2O_3	Cu $(NO_3)_2$. $3H_2O$	0.96	0.1
Cu/γ-Al_2O_3	Cu $(NO_3)_2$. $3H_2O$	1.92	0.2
Cu/γ-Al_2O_3	Cu $(NO_3)_2$. $3H_2O$	2.88	0.3
Cu/γ-Al_2O_3	Cu $(NO_3)_2$. $3H_2O$	3.86	0.4
Cu/γ-Al_2O_3	Cu $(NO_3)_2$. $3H_2O$	4.8	0.5
Cu/Mg/γ-Al_2O_3	$Cu(NO_3)_2$ and $Mg(NO_3)_2$	0.86 and 1.02	0.1/0.1
Cu/Mg/γ-Al_2O_3	Cu $(NO_3)_2$ and $Mg(NO_3)_2$	1.92 and 2.04	0.2/0.2
Cu/Mg/γ-Al_2O_3	Cu $(NO_3)_2$ and $Mg(NO_3)_2$	5.12 and 4.8	0.5/0.5
Ce/γ-Al_2O_3	$Ce(NO_3)_3.6H_2O$	1.74	0.1
Co/γ-Al_2O_3	$Co(NO_3)_2.6H_2O$	5.8	0.5
Mg/Co/γ-Al_2O_3	$Co(NO_3)_2$ and $Mg(NO_3)_2$	5.8 and 5.12	0.5/0.5
Ca/Co/γ-Al_2O_3	$Co(NO_3)_2$ and $CaCl_2$	5.8 and 2.2	0.7/0.5
Cu/Co/γ-Al_2O_3	Cu $(NO_3)_2$ and $Co(NO_3)_2$	4.8 and 5.8	0. 5
Fe/γ-Al_2O_3	$Fe_2(NO_3)_3.9H_2O$	1.62	0.1
Co/γ-Al_2O_3	$Co(NO_3)_2.6H_2O$	1.16	0.1
Fe/Co/γ-Al_2O_3	$Co(NO_3)_2.6H_2O$ and $Fe_2(NO_3)_3.9H_2O$	1.16 and 1.62	0.1

Synthesis of metal doped-alumina by sol-gel precipitation

Alumina and metal doped-alumina have been prepared by a sol-gel method developed previously for pure alumina [25]. 20 g of $Al(O^{sec}Bu)_3$ were poured into a glass vessel containing 2-butoxyethanol (BuOEt) (162 g) under vigorous stirring. Then 0.3 g of dodecylamine (DDA) was added into the mixture solution under stirring. When DDA was fully dissolved, 7.6 mL of water or aqueous metal (Me) salt solutions were added dropwise. The obtained sols were vigorously stirred and kept in static at 40 °C for 24 h. The obtained solids were filtered, washed several times with 2-BuOEt, dried at 80 °C and finally calcined at 600, 750 or 800 °C for 5 h. The molar composition of the mixture is 1 Al / 0.04 DDA/ 5.27 H_2O/ 17 BuOEt/ x Me, x = 0.1 – 0.5 (Table 2).

Table 2. List of metal doped-alumina prepared by sol-gel method for 20 g $Al(O^{sec}Bu)_3$

Catalyst	Metal salt	Metal salt g	Me/Al molar ratio	$T_{calcination}$ °C
Al_2O_3	/	0	/	/
Ti-Al_2O_3	Titanium isopropoxide	6.143	0.25	750
Cu-Mg-Al_2O_3	Cu $(NO_3)_2$ and $Mg(NO_3)_2$	3.91 and 4.15	0.2	600
Cu-Mg-Al_2O_3	Cu $(NO_3)_2$ and $Mg(NO_3)_2$	3.91 and 4.15	0.2	800
Cu-Al_2O_3	Cu $(NO_3)_2$	3.96	0.2	600
Cu-Al_2O_3	Cu $(NO_3)_2$	3.96	0.2	800
Cu-Ca-Al_2O_3	$CaCl_2$ and Cu $(NO_3)_2$	1.82 and 3.96	0.2	600
Cu-Ca-Al_2O_3	$CaCl_2$ and Cu $(NO_3)_2$	1.82 and 3.96	0.2	800
Cu-Mg-Al_2O_3	Cu $(NO_3)_2$ and $Mg(NO_3)_2$	9.9 and 10.5	0.5	600
Ce-Al_2O_3	$Ce(NO_3)_3$. $6H_2O$	3.56	0.1	600

Methods

Basicity measurement by benzoic acid adsorption

Aqueous solutions of different concentrations of benzoic acid (solubility 2.9 g/L or 0.020 mol/L) have been prepared and characterized by UV spectroscopy (Fig. S1). At pH < 2 (adjusted with one drop of HCl), the benzoic acid concentration [C] shows a linear relationship with the maximum intensity (I) of the most intense band at 273 nm:

$$I = 985.011\,[C] - 0.0741$$

This equation was used to determine the amount of benzoic acid remaining in solution after adsorption on the different materials. Typically, 0.035 g of solid was added into 10 mL of 0.002 mol/L benzoic acid solution (pH = 3.3) under vigorous stirring for 4 h to insure adsorption equilibrium (no difference in UV intensity was observed after 2 and 24 h of stirring). Then the solution and the solid were separated by filtration. The pH of the solution was measured and adjusted at pH < 2 value with HCl. The solution is characterized by UV spectroscopy and the concentration of benzoic acid was determined. The amount of benzoic acid adsorbed on the solid was calculated by difference with the initial concentration.

Determination of the oxidative character of the materials

The oxidative dehydrogenation of benzyl alcohol into benzaldehyde (Scheme 1) was chosen as reaction model for determining the oxidative properties of the catalysts prepared by impregnation and sol-gel method.

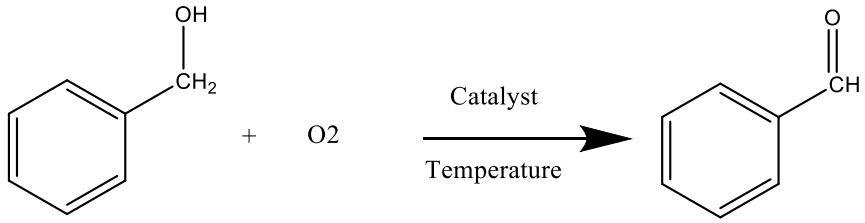

Scheme 1. Catalytic oxidation of benzyl alcohol to benzaldehyde

In a typical oxidation reaction, the catalyst (0.3 g) was dispersed in 15 mL of cyclohexane followed by the addition of benzyl alcohol (517 µL, 4.97 mmol) in an autoclave reactor. The reaction was carried out under stirring for 24 h at 150 °C and air pressure of 2 bar.

Periodically reaction samples were recovered, filtered and analyzed by GC-MS (Agilent, GC-2010) with a ZB-35 HT column. The column temperature increased from 80 to 180 °C with the rate of 15 °C/min, injector temperature was 250 °C, column flow was 20 mL/min. Calibration curves have been plotted between the amount of benzaldehyde/benzyl alcohol and GC area (Fig. S2). The amount of the benzyl alcohol has been taken into account for determining the reaction conversion and the benzaldehyde yield has been calculated. Benzaldehyde is the only product, no traces of benzoic acid have been obtained under these conditions.

Materials Characterization

All measurements were performed at "Plateau Technique, Pole Chimie Balard Montpellier".
X-Ray Diffraction (XRD) patterns of the materials were performed using a Bruker D8 Advance diffractometer with a Bragg-Brentano geometry and equipped with a Bruker Lynx Eye detector. XRD patterns were recorded in the range 10-70° (2θ) to identify the oxide peaks. The angular step size was of 0.0197° and the counting time of 0.2 s per step.
The textural properties of the materials were determined from the N_2 adsorption/desorption isotherms at 77 K measured on a Micromeritics Tristar 3000 apparatus. The samples were previously outgassed in vacuum at 250 °C for 12 h. Mesopore volumes were determined at the end of the condensation step, the surface area by the BET equation and the mesopore diameter by the Broekhoff and de Boer method on the desorption isotherm [31].
Materials morphology was studied using a Hitachi S-4800 I FEG-SEM Scanning Electron Microscope operating at 5 kV at "Plateau Technique de l'IEM laboratoire du Pole Chimie Balard Montpellier". Transmission electron microscopy (TEM) images were acquired on microtomed samples (slices of 70 nm) with a JEOL 1200 EX II instrument operating at 120 kV.
Energy Dispersive Spectroscopy (EDS) chemical analyses (in atomic %) were performed on a FEI Quanta 200F (15 kV) apparatus.

Catalytic ozonation tests

Catalytic ozonation tests have been performed using a synthetic mixture representative of a produced water (water coming naturally during oil or gas extraction) having the following composition: phenol (200 mg/L), acetic acid (200 mg/L), naphtenic acid (25 mg/L), pyrene (0.05 mg/L), naphthalene (0.95 mg/L), NaCl (50 g/L). The solution has a pH of 3.3-4.3, a redox potential of 350 mV, a Total Organic Carbon (TOC) content (or more precisely Non

Purgeable Organic Carbon, NPOC) of 216 mg/L and a Chemical Oxygen Demand (COD) of 668 mgO_2/L.

The ozonation reactions were carried out at 30 °C in a bubble column reactor (7 cm diameter, 25 cm height) (Fig. S3) using 1 L of solution and 5 g of catalyst (previously dehydrated at 105 °C for 16 h). At t = 0 min the flow of ozone was started. Aliquots (8 mL) were taken at t = 5, 10, 15, 20, 30, 60, 90, 120, 150, 180, 240, 300 min. After measuring the concentration of dissolved O_3, the recovered samples were degassed by N_2 bubbling and stored at low temperature for the further analysis. At the end of the catalytic test, the catalyst was recovered by filtration, washed with water and dried 100 °C for further characterizations.

The dissolved ozone concentration was measured by adding a fresh aliquot into an indigo solution [26]. Ozone in acidic solution leads to a rapid discoloration of indigo. The absorbance at 600 nm is directly proportional to the ozone concentration. The absorbance has been measured with a UV-Vis spectrophotometer (Thermoscientific Evolution 201) in a quartz cuvette of 1 cm.

COD measurements were not recorded as too imprecise due to the presence of the high amount of salt.

TOC measurements were performed with a TOCmeter Shimadzu TOC Vppn with a method developed at TOTAL SA (adapted from NF 1484) using acidification at pH 2 and degassing of the sample. Solutions were filtered before analysis (filter 0.45 μm) and diluted 1/10 with water to decrease the alkalinity.

The consumed ozone by oxidized carbon was measured from the difference of concentration of gaseous ozone in the input and in the output of the reactor (Fig. S3). The flow rate of gas in the reactor is known (0.2 L/min), the measurements of ozone concentration in the input and output of the reactor allow to calculate the total ozone mass transferred in the liquid. The dissolved ozone, measured by the indigo method, was subtracted from the total ozone mass to access to the amount of ozone consumed during the chemical reaction. By dividing this amount by the amount of mineralized carbon measured by TOC, the amount of consumed ozone by oxidized carbon has been calculated by the following equation [27]:

$$\frac{O_{3,consumed}}{C_{org,oxidized}} = \frac{\frac{(O_{3,gas,input} - O_{3,gas,output})}{M_{O_3}} t_x Q_g}{C_{org,initial} X(\%) V}$$

with $O_{3,consumed}$ the amount (mol) of consumed ozone during the reaction, $C_{org,oxidized}$ the amount (mol) of organic carbon oxidized during the reaction, $O_{3,gaz,input}$ (g/L) and $O_{3,gas,output}$ (g/L) the amount of ozone in the gas phase in the input and output of the reactor, respectively, t_x (min) the time needed to degrade X% of organic carbon, X percentage of organic carbon degraded, Q_g the gas flow rate (L/min) at the input of the reactor, $C_{org,initial}$ the amount (mol/L) of initial organic carbon, V the reactor volume (L), M_{O3} the molar mass of ozone (48 g/mol).

RESULTS AND DISCUSSION

Materials characterization

Materials prepared by incipient wetness impregnation

The XRD pattern of the parent γ-Al_2O_3 shows three broad peaks at about 37, 46 and 67° corresponding to a cubic spinel with defects (Fig. 1). The same crystallographic structure was observed for the Mg/γ-Al_2O_3 materials prepared with molar ratio 0.025 < Mg/Al < 0.1 and calcined at 600 °C. For the higher amount of Mg (Mg/Al = 0.2) a slight shift of XRD peaks towards lower angles is observed suggesting the incorporation of Mg in the spinel structure of γ-Al_2O_3 leading to $Mg_xAl_{2-x}O_4$ phase. N_2 adsorption-desorption isotherms (77 K) of γ-Al_2O_3 and Mg/γ-Al_2O_3 samples (0.025 < Mg/Al < 0.2) are similar (Fig. 1, Table 3). All Mg/γ-Al_2O_3 materials featured mesopore diameters of 10-11 nm, mesopore volumes around 0.6 mL/g and specific surface areas around 230-260 m^2/g. These results show that the incorporation of Mg in γ-Al_2O_3 did not affect the textural characteristics of γ-Al_2O_3.

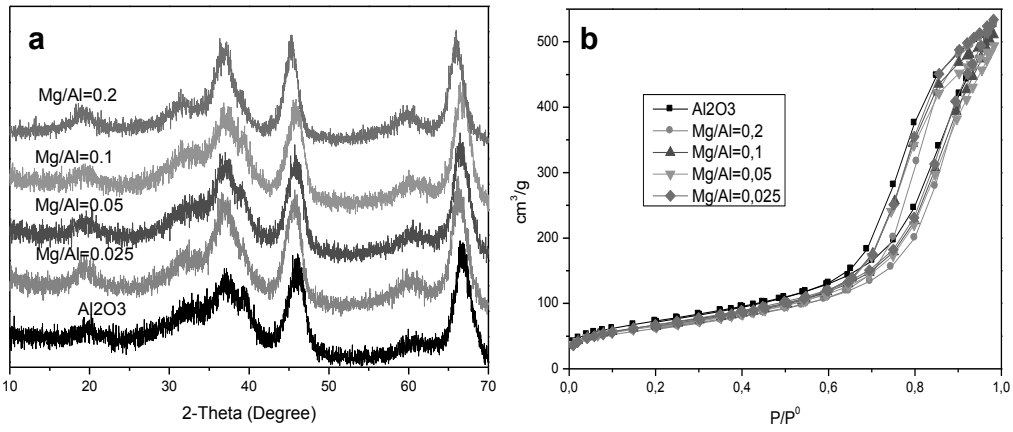

Figure 1. (a) XRD patterns and (b) nitrogen sorption isotherms at 77 K of γ-Al_2O_3 and Mg/γ-Al_2O_3 samples prepared by incipient wetness impregnation with different Mg/Al molar ratios and calcined at 600°C.

Table 3. Textural properties determined from N_2 sorption isotherms at 77 K of catalysts before and after ozonation: γ-Al_2O_3, Cu/γ-Al_2O_3, Mg/γ-Al_2O_3 and Mg/Cu/γ-Al_2O_3 synthesized by incipient wetness impregnation and sol-gel (sg) and calcined at 600 °C.

Materials	$Ø_{pore}$ (nm)	V_{total} (ml/g)	S_{BET} (m²/g)	C_{BET}
γ-Al_2O_3	12.2	0.58	183	135
γ-Al_2O_3 (600°C)	10.8	0.69	221	122
after 1 ozonation	14.0	0.43	146	146
Cu/Al = 0.2	11.5	0.55	195	102
after 1 ozonation	14.0	0.43	140	126
Mg/Al = 0.1	11.9	0.69	259	119
after 1 ozonation	14.0	0.59	193	168
after 2 ozonations	14.0	0.60	195	155
Mg/Cu/Al = 0.2 sg	6.5	0.44	297	115
after 1 ozonation	2 and 30 nm	0.03	19	92
Mg/Al = 0.2	11.4	0.60	240	120
after 1 ozonation	13.0	0.53	179	156

For Mg/γ-Al_2O_3 (Mg/Al = 0.05), the calcination temperature from 450 to 750 °C does not affect the crystalline structure (Fig. S4). Only slightly thinner peaks are observed for a calcination temperature of 750 °C resulting from some particle sintering. Consequently, the increase of calcination temperature leads to a slight decrease in specific surface area from 246 to 196 m^2/g, a slight increase of mesopore diameter from 10 to 11 nm and mesoporous volume from 0.56 to 0.64 mL/g. This is consistent with the same behavior observed for γ-Al_2O_3 in this temperature range.

XRD patterns of Ca/γ-Al_2O_3 and Ba/γ-Al_2O_3 with M/Al = 0.05 calcined at 600 °C (Fig. S5) show the same peak positions as γ-Al_2O_3 or Mg/γ-Al_2O_3 (Mg/Al = 0.05), but with a decrease in peaks intensity suggesting a decrease in crystallinity when the ionic radius of the cation increases (Ba > Ca > Mg). This suggests that the incorporation of these cations into the spinel structure of γ-Al_2O_3 induces a larger deformation for the larger cation (Ba). The incorporation of Ba and Ca in γ-Al_2O_3 does not affect the textural properties (Table S1), which remain close to those of γ-Al_2O_3.

XRD patterns (Fig. S6) of M/γ-Al_2O_3 samples with M/Al = 0.05 calcined at 600 °C for M = Fe, Co, Ni, Cu, Zn, Zr, Ce show globally the same crystallographic structure as γ-Al_2O_3. XRD patterns of Fe/, Co/, Ni/, Zn/γ-Al_2O_3 are similar to γ-Al_2O_3 crystallographic structure suggesting the incorporation of these cations in the spinel structure of γ-Al_2O_3 with slight decrease in crystallinity in the order Zn > Ni > Co > Fe. These cations are known to form MAl_2O_4 spinel phases at high temperature. XRD patterns of Cu/, Zr/, Ce/γ-Al_2O_3 show additional peaks suggesting the formation of oxides nanoparticles (NPs) at the surface of γ-

Al_2O_3. For Zr/γ-Al_2O_3 an additional broad peak at 2Θ = 30° suggests the formation of some tiny ZrO_2 NPs at the surface of γ-Al_2O_3. Similarly for Ce and Cu additional peaks corresponding to oxide NPs are observed. Peaks at 29 and 57° in 2Θ for Ce/γ-Al_2O_3 are characteristic of CeO_2 NPs and peaks at 36 and 39° in 2Θ for Cu/γ-Al_2O_3 are characteristic of CuO NPs with monoclinic structure.

The impregnation with Co on γ-Al_2O_3 for a larger amount of Co (Co/Al = 0.5) leads to additional XRD peaks (Fig. S7) appearing at 2Θ = 32, 37, 45, 59, 66° characteristic of Co_3O_4 NPs formation at the surface of spinel Co/γ-Al_2O_3 leading to a decrease of surface area and mesopore volume (Table S2). A co-addition of Mg, Ca or Fe with Co does not change the XRD patterns, whereas a co-addition of Cu leads to the formation of supplementary CuO NPs. N_2 adsorption-desorption isotherms of the different elements (Fe, Co, Ni, Cu, Zn, Ce, Zr with M/Al = 0.05) deposited on γ-Al_2O_3 show little variation of textural properties of γ-Al_2O_3 except for Ce/γ-Al_2O_3, which shows a decrease of surface area and mesopore volume suggesting the blocking of some mesopores by CeO_2 NPs, while CuO NPs does not affect textural properties of γ-Al_2O_3 (Table S3).

The increase of Cu/Al ratio 0.1 < Cu/Al < 0.5 during the impregnation on γ-Al_2O_3 (calcination at 600 °C) leads to the increase of XRD peaks intensity of CuO NPs (Fig. 2) at the surface of γ-Al_2O_3. For Cu/Al ≤ 0.2 the textural properties of γ-Al_2O_3 are maintained, whereas for larger amount of Cu, CuO NPs are blocking the entrance of some mesopores leading to a decrease of surface area and mesopore volume of the materials (Table S4). CuO NPs are of interest as they are known for their oxidative properties [29]. The increase of calcination temperature to 800 °C leads to the appearance of a well crystalline phase, a cubic spinel phase $CuAl_2O_4$ [30] for Cu/Al ≤ 0.3 and for Cu/Al ≥ 0.4 in addition to the spinel phase some CuO NPs (Fig. S8). We can suggest that for a calcination at 600 °C the CuO NPs are at the surface of a spinel phase $Cu_xAl_{2-x}O_4$. The increase of temperature at 800 °C lead the increase of crystallinity and to the change of textural properties of the Cu/γ-Al_2O_3 materials (Table S5) with a drastic decrease in surface area from 200 m^2/g to 100 and 40 m^2/g for Cu/Al ≤ 0.2 and 0.3 ≤ Cu/Al ≤ 0.5, respectively. It is to notice that spinel-type materials $CuAl_2O_4$ and $CuMgAl_2O_4$ have already been used efficiently in catalytic ozonation for the degradation of clofibric acid, a blood lipid regulator [31].

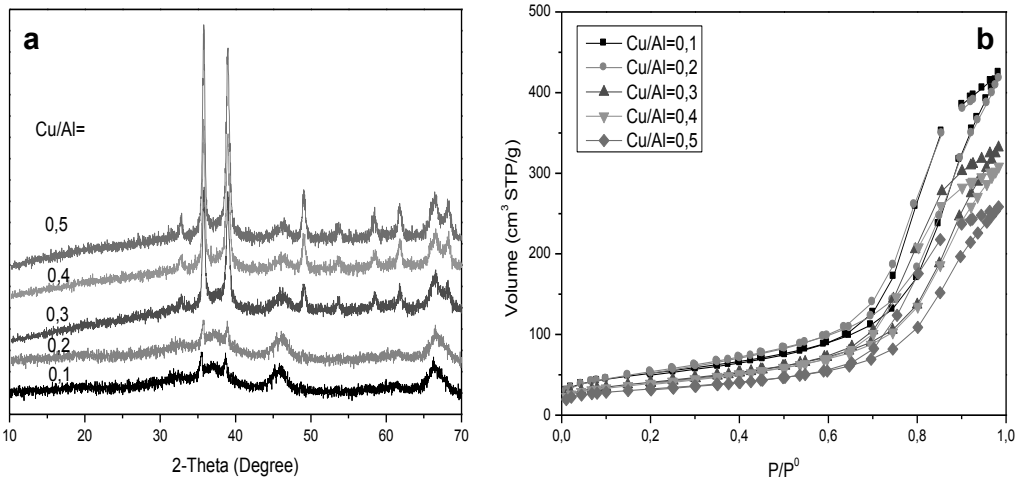

Fig. 2. (a) XRD patterns and (b) nitrogen sorption isotherms at 77 K of Cu/γ-Al_2O_3 samples prepared by incipient wetness impregnation with different Cu/Al molar ratios and calcined at 600 °C.

Mixed metals Mg and Cu have been co-impregnated on γ-Al_2O_3. For a calcination at 600 °C, the increase of Mg/Cu/Al molar ratio from 0.1/0.1/1 to 0.2/0.2/1 and 0.5/0.5/1 leads to an increase of XRD peaks intensity of CuO NPs (Fig. 3) revealing the increase of the amount of CuO NPs at the surface of Mg/γ-Al_2O_3. The peak intensities corresponding to CuO NPs are higher than for the materials prepared with Cu alone on γ-Al_2O_3 (Fig. 2). This suggests that Mg is preferred to Cu to enter in γ-Al_2O_3 spinel structure, and consequently leads to the formation of larger CuO NPs at the surface of Mg/γ-Al_2O_3 spinel phase. Consequently, surface area and mesopore volume are slightly lower for Cu/Mg/Al materials in comparison to Cu/Al materials with surface areas of 153 instead of 195 m^2/g for Cu/Al = 0.2 and 97 instead of 116 m^2/g for Cu/Al = 0.5 (Table S6).

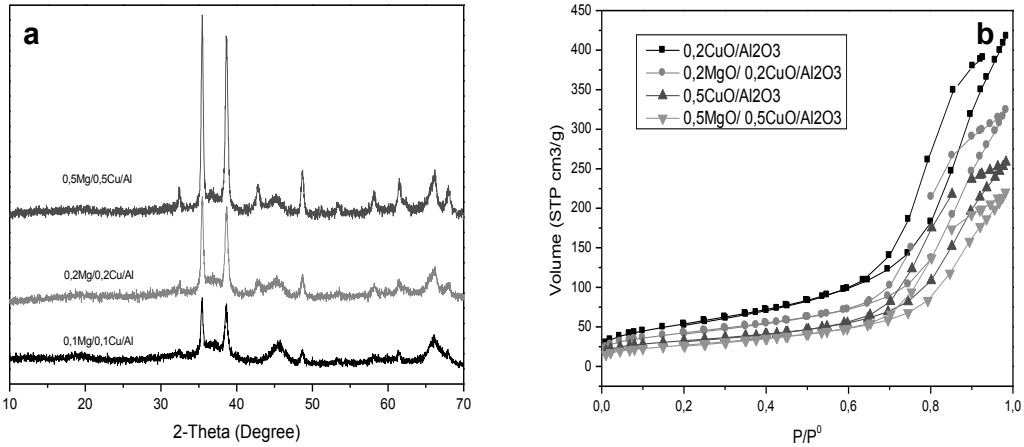

Fig. 3. (a) XRD patterns and nitrogen sorption isotherms at 77 K of Mg/Cu/γ-Al_2O_3 samples prepared by incipient wetness impregnation with different molar ratios and calcined at 600 °C.

Materials prepared by sol-gel

XRD patterns of Al_2O_3 synthesized by sol-gel method and calcined at different temperatures (Fig. S9) show that at 600 °C alumina exhibits a poorly crystallized gamma structure. A temperature higher than 750°C is necessary to reach the gamma crystalline phase of alumina. Alumina synthesized by the sol-gel method and calcined at 600 °C features high surface area, mesopore volume and mesopore diameter of 440 m^2/g, 0.84 mL/g and 7 nm, respectively (Table S7). The increase of calcination temperature to 800 °C to reach γ-Al_2O_3 structure leads to a decrease of surface area and mesopore volume to 233 m^2/g and 0.65 mL/g, respectively, similar to commercial γ-Al_2O_3 used for impregnation.

The sol-gel method has been applied to synthesize metal doped-alumina materials. A Ti/Al_2O_3 material has been synthesized with a Ti/Al molar ratio of 0.25. TiO_2 is generally known for its high oxidative character, especially when it features the anatase crystalline phase. However, the resulting mixed oxides is mostly amorphous and the gamma alumina phase is not well crystallized even for a calcination at 750 °C (Fig. S10). The mixed-oxide Ti/Al_2O_3 synthesized by sol-gel presents very different textural properties in comparison to alumina: small mesopore diameter of 5 nm, a low mesopore volume of 0.27 mL/g and a surface area of 240 m^2/g (Table S8).

Cu/Al_2O_3 (Cu/Al = 0.2) materials have been prepared by sol-gel and calcined at 600 and 800 °C. XRD pattern (Fig. S11) of the material calcined at 600 °C shows mainly an amorphous phase with two weak peaks at 2Θ = 35 and 40° due to few CuO NPs. The textural properties of Cu/Al_2O_3 calcined at 600 °C (Table S9) are close to the one of Ti/Al_2O_3. An increase of calcination temperature to 800 °C reveals the formation of a cubic spinel phase $CuAl_2O_4$ (Fig. S11). The addition of Mg (Mg/Al = 0.2) to form a mixed Cu/Mg/Al (0.2/0.2/1) material leads after calcination at 600 °C to more crystallized CuO NPs (Fig. S12). This observation is similar to that made for the Cu/Mg/Al (0.2/0.2/1) material obtained by impregnation due to the preferential formation of Mg/Al_2O_3 spinel phase. This material shows a higher mesopore volume (0.44 mL/g) and surface area (300 m^2/g) (Table S10) in comparison to Ti/Al_2O_3 and Cu/Al_2O_3 materials prepared by sol-gel. By increasing the amount of Mg and Cu (Cu/Mg/Al = 0.5/0.5/1) the amount of CuO NPs increases evidenced by the increase of the intensity of XRD peaks (Fig. S12). Nitrogen sorption isotherm shows the formation of less homogeneous size distributions of mesopores suggesting inhomogeneous sizes of NPs. The addition of Ca instead of Mg (Cu/Ca/Al = 0.2/0.2/1) leads to the formation of CuO NPs (Fig. S13) and a

drastic loss of the textural properties with a decrease of surface area to 74 m^2/g (Table S11). Ca is presumably more prone to form $CaAl_2O_4$ spinels in comparison to Mg. The increase of calcination temperature to 800 °C, leads to a mixture of poorly crystallized spinel phase and some CuO NPs.

Basicity of the materials in water

The basicity of all materials prepared either by incipient wetness impregnation or by sol-gel precipitation has been investigated. Basic sites can be analyzed in the gas phase for example by CO_2 adsorption monitored by FTIR as we have done in the previous publication using γ-Al_2O_3 for catalytic ozonation [13]. However to be closer to the experimental conditions, a method has been developed to characterize the basicity of the materials in water. In literature a method to analyze the basicity of solids in aqueous medium has been proposed based on the amount of benzoic acid adsorbed measured by UV detection at a wavelength of 272 nm [32]. Authors relate the amount of benzoic acid adsorbed on the solids to the effective amount of basic sites: the higher amount adsorbed means the higher number of basic sites in the materials. Benzoic acid is also an interesting molecule for the present study as it is representative of carboxylic acids resulting from ozonation of petrochemical pollutants, which in final stage leads mainly to acetic acid and some oxalic and formic acids. Benzoic acid adsorption allows to probe the basicity of materials and in the same time the capacity of the materials to adsorb carboxylic acids. In non-saline petroleum effluents, carboxylic acids were adsorbed on the basic sites of γ-Al_2O_3 leading to a progressive decrease of activity of the catalyst after each run [13]. γ-Al_2O_3 should be reactivated at 600°C to recover its catalytic properties. It is therefore advantageous to develop catalysts, which do not adsorbed carboxylic acids.

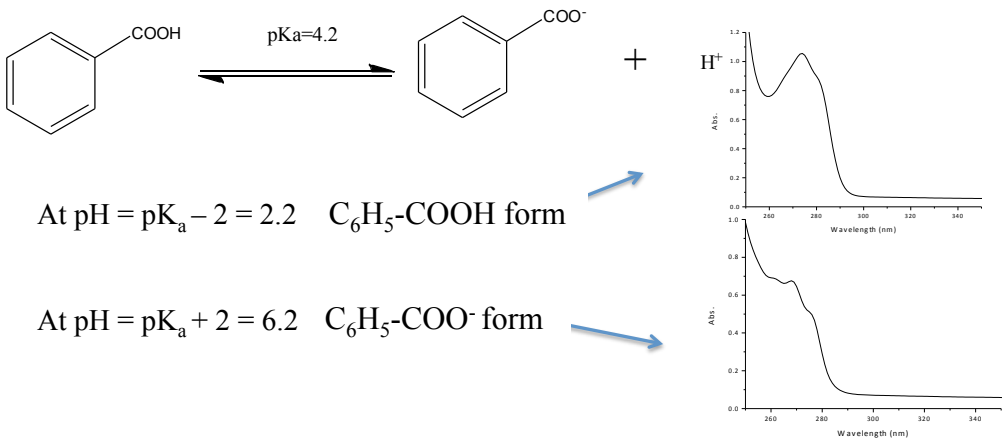

Scheme 2. Example of UV spectra of benzoic acid obtained in acidic and basic conditions

However, interpretation of the UV spectrum of benzoic acid in a water solution is not straightforward since peaks intensity and position vary with the pH of the solution and cannot be solely examined at 272 nm. At a basic pH, the UV bands are shifted towards lower wavelengths and the extinction coefficient of the band decreases resulting in a difficult quantification of benzoic acid in solution. The pKa of benzoic acid is 4.2. At pH < pKa - 2, therefore pH = 2.2, benzoic acid is under its protonated molecular form C_6H_5-COOH, and at pH > pKa + 2, therefore pH = 6.2, benzoic acid is under its anionic form C_6H_5-COO^-. For 2.2 < pH < 6.2, there is an equilibrium between these two forms. The shape of the UV spectrum of the remaining benzoic acid in solution is complex (Scheme 2). For accurate quantitative estimation of the benzoic acid remaining in solution after separation from the solid, it is necessary to adjust the pH below 2.2 or above 6.2 to analyze always the same state of benzoic acid.

We have therefore developed a new methodology to quantify precisely the amount of benzoic acid remaining in solution by UV-Vis measurements to characterize the basicity of the materials and the amount of benzoic acid adsorbed in the solid. First the pH of the benzoic acid solution in contact with the solid has been measured, then the pH of the solution (after filtration) has been decreased below pH 2 to obtain the same position of UV bands, the intensities of the bands were then solely dependent on the benzoic acid concentration.

Basicity of doped-alumina prepared by incipient wetness impregnation

The initial pH of the benzoic acid solution was 3.3. By adding γ-Al_2O_3, the pH increased to 4. At pH = 4 there was a mixture of C_6H_5-COOH and C_6H_5-COO^- and the surface of γ-Al_2O_3 had a majority of Al-OH species with few Al-O^- groups. Benzoic acid was adsorbed on the alumina surface with an amount of 0.37 mmol/g due mainly to Al-OH/C_6H_5-COOH interactions. The addition of Mg/γ-Al_2O_3 materials in the benzoic solution led to an increase of pH values from 5 to 8 depending on Mg amount. The pH of the solution increased with the increase of Mg content and in parallel benzoic acid adsorption decreased with no adsorption observed for Mg/Al > 0.06 (Fig. S14, Table S12). The pH of the solutions were 6.6 and 8.1 for Mg/Al = 0.1 and 0.2, respectively (Fig. 4, Table S12). The basic character of γ-Al_2O_3 was therefore improved by the incorporation of Mg on γ-Al_2O_3. As no adsorption of benzoic acid was observed for Mg/Al > 0.06, Mg/γ-Al_2O_3 materials should prove effective for sustainable

catalytic ozonation. The increase of pH of the benzoic solution is related to the increase of basicity of the materials and is accompanied by a decrease of benzoic acid adsorption (Fig. S15), which is the opposite of what was suggested in literature [32]. In literature [32], nitrogen-doped porous carbons have been studied, which are weakly basic materials leading presumably to no pH increase. In this case the maximum benzoic acid adsorption was found for the more basic materials as only C-N/C_6H_5-COOH interactions are involved. When the pH increases above a value of 4, the amount of C_6H_5-COO^- increases, leading to less adsorption of benzoic acid due to electrostatic repulsion with Al-O^- groups on the surface.

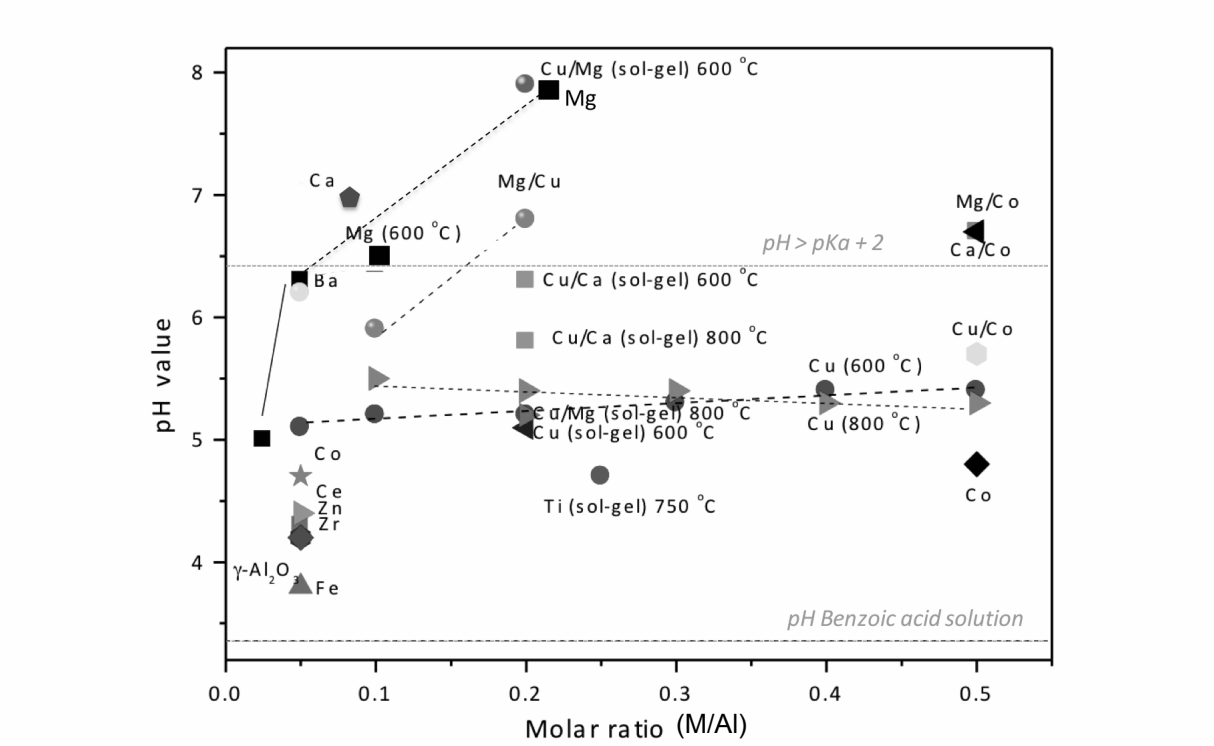

Fig. 4. Basicity test: pH of remaining benzoic acid solution after 4 h contact with metal-doped aluminas materials.

The influence of the calcination temperature on the basic properties have been examined for materials prepared with Mg/Al = 0.05. Whereas materials calcined at temperatures of 450 and 600 °C allowed to increase the pH of the solution to 6.2 and 6.3, respectively, calcination at 750 °C eliminated the promoting effect of Mg on the basicity of alumina, leading to a solution pH of 4.3. Consequently, the amount of adsorbed benzoic acid increased to 0.25 mmol/g as more molecular protonated form of benzoic acid was present (C_6H_5-COOH). This amount of adsorbed benzoic is close and slightly inferior to the one obtained for γ-Al_2O_3, which gives a pH of benzoic acid solution of 4.0. We can suggest that up to a calcination temperature of 600 °C, Mg remains at the surface of γ-Al_2O_3 to form a basic mixed-oxide whereas at 750 °C Mg migrates inside the particle leading to a surface similar to γ-Al_2O_3.

Materials prepared with other alkaline-earth metals (Ba, Ca) (M/Al = 0.05) deposited on γ-Al_2O_3 led to an increase of the pH values of the benzoic acid solution (Fig. 4, Table S12) with the highest pH found for Ca/γ-Al_2O_3 (pH = 7.0). All the pH values of benzoic solutions were above 6.2 for Mg/, Ca/ and Ba/γ-Al_2O_3 materials and benzoic acid was under its anionic form C_6H_5-COO^-. It means that alkaline-earth metals really improve the basicity of γ-Al_2O_3. For Mg/, Ca/ and Ba/γ-Al_2O_3 materials, no benzoic acid was adsorbed on these materials. (Fig. 4, Fig. S14, Table S12).

Besides alkaline-earth metal, other elements (Fe, Co, Ni, Cu, Zn and Ce) have been deposited on γ-Al_2O_3 and calcined at 600 °C. The pH values of the resulting solutions with their mixture with benzoic acid solutions were higher (4.2 < pH < 5.4) than γ-Al_2O_3 (pH = 4.0) except for Fe/γ-Al_2O_3, which pH was 3.8 (Fig. 4, Table S12). Among the series Co/, Ni/, Cu/, Zn/, Ce γ-Al_2O_3, the highest pH values were obtained for Cu/γ-Al_2O_3 with pH = 5.1 to 5.4 for Cu/Al = 0.05 to 0.5, respectively. Co/, Zn/, Cu/γ-Al_2O_3 materials adsorbed a similar amount of benzoic acid (0.23 mmol/g), slightly less than on γ-Al_2O_3 (0.37 mmol/g) (Fig. S14, Table S12). Similarly Ce and Zr deposited on γ-Al_2O_3 show a small increase of pH of the benzoic acid solution with pH = 4.35 for Ce/γ-Al_2O_3 and pH = 4.22 for Zr/γ-Al_2O_3 and lead to an amount of benzoic acid adsorbed of 0.27-0.28 mmol/g. These results are in accordance with the relationship between the pH of solution and the adsorbed benzoic acid amount (Fig. S15) correlated to the amount of anionic form of benzoic acid, which increases with the increase of pH accordingly to its pKa value. An exception is observed for Fe/γ-Al_2O_3, which shows a slight decrease of pH (pH = 3.8) in comparison to γ-Al_2O_3 (pH = 4.0), and no adsorption of benzoic acid (Fig. S15). We suggest that Fe interacts and covers the basic sites of γ-Al_2O_3. Cu/γ-Al_2O_3 features the highest basicity among non alkaline-earth metals deposited on γ-Al_2O_3, but its basicity remains below alkaline-earth/γ-Al_2O_3 as Mg/γ-Al_2O_3 with pH of benzoic acid equal to 8.1 for Mg/Al = 0.2 (Fig. 4, Table S12). Increasing the temperature of calcination to 800 °C for Cu/γ-Al_2O_3 does not decrease the pH (pH = 5.4) as for Mg/γ-Al_2O_3 (pH = 4.3), meaning that Cu remains in the surface of the particles, but the amount of adsorbed benzoic acid decreases to 0.10 mmol/g. This is due to the decrease of the specific surface area of the material coming from the formation of dense spinel $CuAl_2O_4$ phase at 800 °C (Fig. 4, Table S12).

The materials formed by co-impregnation of Mg and Cu on γ-Al_2O_3 with molar ratios Mg/Cu/Al = 0.1/0.1/1 and Mg/Cu/Al = 0.2/0.2/1 show an increase of the pH of the benzoic acid solution with values of 5.9 and 6.8, respectively, which are intermediate of those of Mg/γ-Al_2O_3 (pH = 6.6 and 8.1 for Mg/Al = 0.1 and 0.2, respectively) and those of Cu/γ-Al_2O_3 (pH = 5.2 for Cu/Al = 0.1 and 0.2). The amount of benzoic acid adsorbed is low (0.05 mmol/g) for Mg/Cu/Al = 0.1/0.1/1 and no adsorption of benzoic acid is measured for Mg/Cu/Al = 0.2/0.2/1 (Fig. S14, Table S12) as expected for such pH values (Fig. S15).

In summary, the materials prepared by incipient wetness impregnation featuring the highest basicity are Mg/γ-Al_2O_3 (Mg/Al = 0.2) > Ca/γ-Al_2O_3 (Ca/Al = 0.07) > Mg/Cu/γ-Al_2O_3 (Mg/Cu/Al = 0.2/0.2/1) > Mg/γ-Al_2O_3 (Mg/Al = 0.12). In suspension in benzoic acid solution they lead to pH values higher than 6.2 (Fig. 4) with no benzoic acid adsorption (Fig. S15). These materials are therefore suitable catalysts for sustainable ozonation.

Basicity of the materials prepared by sol-gel

The basicity of alumina and different metal/alumina-based materials prepared by sol-gel precipitation was probed following the same protocol as above.

Similar amounts of benzoic acid were adsorbed on the commercial γ-Al_2O_3 and the sol-gel Al_2O_3 (0.37 mmol/g compared to 0.33 mmol/g) (Table S12). The pH value of the benzoic acid solution after mixing with sol-gel Al_2O_3 was slightly higher (pH = 5) than that obtained with the commercial γ-Al_2O_3 (pH = 4).

The benzoic acid solution in contact with the sol-gel Ti/Al_2O_3 featured a slightly lower pH value (pH = 4.7) than that attained with sol-gel alumina and showed a lower amount of benzoic acid adsorbed (0.18 mmol/g). The sol-gel Cu/Al_2O_3 (Cu/Al = 0.2) led to a pH value (pH = 5.2) similar to that observed with the sol-gel alumina and the Cu/γ-Al_2O_3 prepared by impregnation with a slightly lower amount of benzoic acid adsorbed (0.19 mmol/g) (Table S12). The highest basicity was reached with the sol-gel Cu/Mg/Al_2O_3 with a pH of benzoic acid solution of 7.9, close to the one obtained for the more basic material prepared by impregnation (Mg/γ-Al_2O_3 with Mg/Al = 0.2; pH = 8.1) (Fig. 4), and a low amount of benzoic acid adsorbed (0.06 mmol/g).

As shown above, most of metal-doped alumina materials prepared either by incipient wetness deposition or by sol-gel (sg) method increased the basicity of alumina. (Fig. 4, Fig. S14). The highest basicity was revealed by the materials containing alkaline-earth metals. The basicity decreases in the following order: Mg/γ-Al_2O_3 (Mg/Al = 0.2) ≥ Mg/Cu/Al_2O_3 (sg) (Mg/Cu/Al = 0.2/0.2/1) > Ca/γ-Al_2O_3 (Ca/Al = 0.07) > Mg/Cu/γ-Al_2O_3 (Mg/Cu/Al = 0.2/0.2/1) > Mg/γ-Al_2O_3 (Mg/Al = 0.12). The basicity brought by the transition metals is lower and it decreases in the order: Cu > Co > Ce > Zn > Ni = Zr > Fe.

Oxidative character of the materials

As a test for scaling the oxidative character of the materials, we have chosen a catalytic model reaction consisting in the oxidative dehydrogenation of benzyl alcohol into benzaldehyde in the presence of air [29]. In literature [29], the reaction was performed at 100 °C for 24 h under atmospheric pressure of air, using CuO NPs as catalyst in toluene with 0.33 mol/L of benzyl alcohol and 20 g/L of catalyst, corresponding to 75 mol% Cu with respect to benzyl alcohol. CuO NPs were synthesized from $CuCl_2.2H_2O$ in water in presence of N-cyclohexyl-3-amino-propane sulfonic acid as chelating agent with pH adjustment at 11 with KOH, afforded, after washing and drying, a high benzaldehyde yield (> 99% conversion and selectivity).

First, the reaction conditions (solvent, catalyst amount, reaction time, temperature, air pressure) were optimized with the material prepared by incipient wetness impregnation consisting of CuO NPs supported on γ-Al_2O_3 and calcined at 600 °C, Cu/γ-Al_2O_3 (Cu/Al = 0.2). Toluene as the solvent can be oxidized into benzaldehyde and therefore it was replaced by cyclohexane. Without catalyst, benzyl alcohol could also be converted into benzaldehyde with 6% conversion for air pressure superior to 2 bar. The air pressure was therefore set at 2 bar. The highest conversion of benzyl alcohol conversion into benzaldehyde was obtained with 0.3 g of catalyst in 15 mL (20 g/L) of cyclohexane for 4.97 mmol of benzyl alcohol (0.33 mol/L), for a reaction temperature of 150 °C and a reaction time of 24 h. Benzaldehyde was the only product obtained, no traces of benzoic acid was detected.

The oxidative properties of all the materials have been evaluated using the optimal conditions defined above for Cu/γ-Al_2O_3 (Cu/Al = 0.2). Benzaldehyde yields are reported in Fig. 5 for all alumina-based materials prepared by incipient wetness impregnation and sol-gel method. The highest benzaldehyde yields were obtained on copper containing materials prepared by

incipient wetness impregnation on γ-Al_2O_3 and calcined at 600 °C. In the case of Cu/γ-Al_2O_3 materials, the benzaldehyde yield increased to 68% when the molar ratio Cu/Al increased from 0.1 to 0.2. Further increase of the amount of Cu on γ-Al_2O_3 (Cu/Al = 0.4 and 0.5) had an unfavorable effect on the catalytic activity with a decrease of benzaldehyde yield to 30 %. This is probably due to an increase in size of the CuO NPs by sintering, leading to a smaller intrinsic surface area of the NPs.

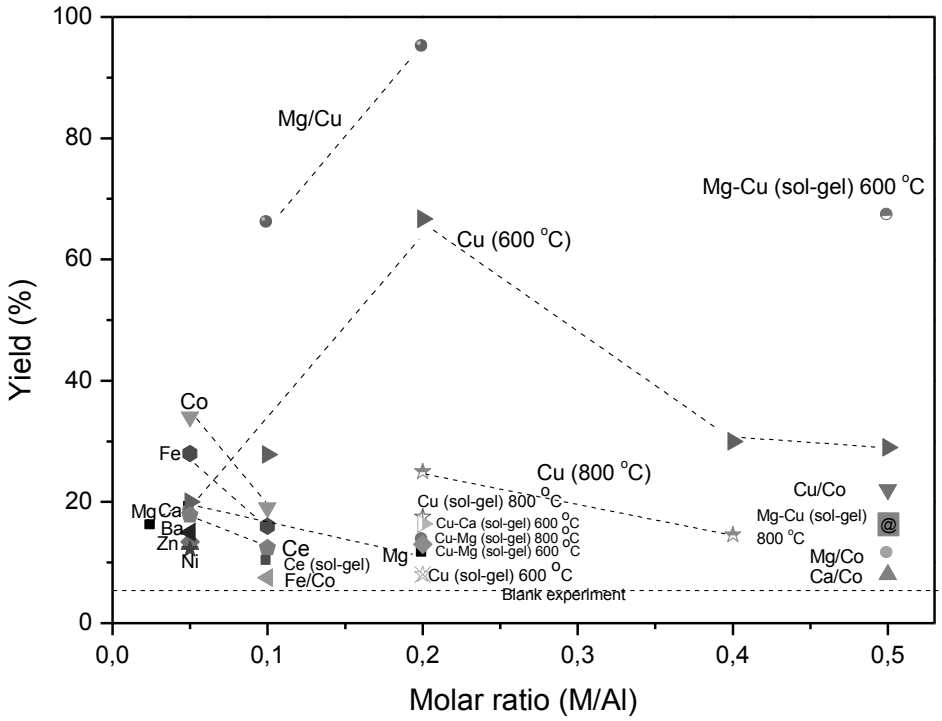

Fig. 5. Oxidation test: yields of benzaldehyde with the different M/Al_2O_3 catalysts. The reaction condition: benzyl alcohol (517 µL), cyclohexane (15 mL), 0.3 g catalyst, 150 °C for 24 h, under air 2.0 bar.

Interestingly and surprisingly, the materials prepared by co-impregnation of Cu and Mg, Mg/Cu/γ-Al_2O_3 (Mg/Cu/Al = 0.1/0.1/1 and 0.2/0.2/1) led to higher benzaldehyde yields of 68 and 95%, respectively (Fig. 5). As explained above, Mg is more prone than Cu to enter in γ-Al_2O_3 spinel structure and consequently leads to the formation of larger size CuO NPs at the surface. However, in this case the growth of the size of the NPs has a favorable impact on the catalytic activity. This indicates that the support for CuO NPs plays a role in the reaction. The strong interaction between a strongly basic support, which is electron donor, as Mg/γ-Al_2O_3, with CuO NPs prevents their migration on the surface and their sintering. The higher activity is presumably due to a better dispersion of CuO NPs at the surface of Mg/γ-Al_2O_3 in comparison to γ-Al_2O_3. Mg/γ-Al_2O_3 mixed-oxides are often preferred to γ-Al_2O_3 as supports

for metal NPs in catalysis as they bring a structural promoting role towards interaction with the active metal allowing higher metal dispersion by stabilizing smaller nanoparticles [33-37].

To conclude, the materials with the highest oxidative character are Mg/Cu/γ-Al_2O_3 (Mg/Cu/Al = 0.2/0.2/1) > Mg/Cu/γ-Al_2O_3 (Mg/Cu/Al = 0.1/0.1/1) = Cu/γ-Al_2O_3 (Cu/Al = 0.2). Notably, Mg/Cu/γ-Al_2O_3 (Mg/Cu/Al = 0.2/0.2/1) features both high oxidative character and high basicity.

Catalytic ozonation

Reaction mechanisms

The mechanism of ozonation has been investigated in previous works [13, 38] using various model substrates in the presence or absence of catalyst. Main results are summarized in Tables 4 and 5. With 2,4-dimethylphenol (DMP) as starting substrate, intermediate molecules have been identified, and final by-products consisted of acetic acid > formic acid >> oxalic acid.

Acetic acid is formed rapidly similarly for single and catalytic ozonation, though in lower amount in the presence of catalyst. Acetic acid is the main final product as it cannot be oxidized by O_3 or HO°. The use of catalysts significantly increases the efficiency of the ozonation process as illustrated in runs 1, 4, 7 and 9, Table 4. For γ-Al_2O_3 initial rate of degradation is increased by a factor 5.3 and TOC removal by a factor 3 to 4. This is due to the occurrence of the radical pathway, as evidenced by the addition of OH° scavengers such as NaCl and t-butanol in the reaction medium (runs 5, 6 and 8, Table 4). In both cases the initial rate of TOC removal is significantly decreased as well as the final extent of TOC removal. For γ-Al_2O_3 initial rate of degradation is decreased by a factor 2.2 and TOC removal by a factor 1.6. Without scavengers, phenol removal results from direct ozonation with O_3, from reaction with OH° radicals and from adsorption of by-products on the catalyst in the case of γ-Al_2O_3. FTIR and ^{13}C MAS NMR experiments demonstrated that the active catalytic sites of γ-Al_2O_3 are surface basic sites.

The use of scavengers allowed to determine the initial rate of degradation for each mechanism: for the mixed mechanism O_3 + HO° + adsorption (γ-Al_2O_3) the initial rate of degradation was 5.3 times higher than for a mechanism with O_3 alone, and the mixed mechanism O_3 + adsorption (γ-Al_2O_3 + scavenger) was 2.4 times higher than direct O_3 ozonation.

Table 4. Ozonation of 2,4-dimethylphenol. (Temperature : 25 °C, O_3 flow rate : 40 L/h, Inlet O_3 concentration : 2 g/Nm^3, [2,4-DMP] = 50 ml/L, Solution volume : 1.5 L)

Run #	Catalyst	Radical scavenger	Relative initial reaction rate	% TOC removal after 300 min	Ref.
1	None	None	1	14	38
2	None	NaCl (50 g/L)	0.7	10	38
3	None	t-BuOH (25 mg/L)	0.8	12	13
4	Na-LTA (2 g/L)	None	4.0	34	38
5	Na-LTA (2 g/L)	NaCl (50 g/L)	0.9	12	38
6	Na-LTA (2 g/L)	t-BuOH (25 mg/L)	1.3	15	38
7	γ-Al_2O_3 (2 g/L)	None	5.3	47	13
8	γ-Al_2O_3 (2 g/L)	t-BuOH (25 mg/L)	2.4	30	13
9	γ-Al_2O_3 (5 g/L)	None	5.3	57	13

In the case of the synthetic effluent simulating produced water from off-shore oil extraction (phenol (200 mg/L), polycyclic aromatic hydrocarbons (PAHs) as naphtenic acid (25 mg/L), pyrene (0.05 mg/L) and naphthalene (0.95 mg/L), acetic acid (200 mg/L)), the use of γ-Al_2O_3 as catalyst resulted in a strong (6.4 fold) increase of the initial rate of TOC removal (runs 10 and 12, Table 5) compared to direct ozonation, as observed with the DMP substrate. The mechanism is therefore similar and is a mixed mechanism O_3 + HO° + adsorption (γ-Al_2O_3). In both systems (direct and catalytic ozonation), however, the extent of TOC removal limits at 50-60%, due to the high initial content of refractory acetic acid in the starting solution.

Table 5

Ozonation of petroleum model effluent. (Temperature 35°C, O_3 flow rate : 24 L/h, Inlet O_3 concentration : 5 g/ Nm^3, Solution volume : 1.5 L, [Phenol] : 200 mg/L, [Naphtenic acid] = 50 mg/L, [Pyrene] = 0.05 mg/L, [Naphtalene] = 0.95 mg/L, [Acetic Acid] = 200 mg/L)

Run #	Catalyst	Radical scavenger	Relative initial reaction rate	% TOC removal after 300 min	Ref.
10	None	None	1	59	13
11	None	NaCl (50 g/L)	0.7	95	13
12	γ-Al_2O_3 (5 g/L)	None	6.4	52	13
13	γ-Al_2O_3 (5 g/L)	NaCl (50 g/L)	3.8	92	13
14	γ-Al_2O_3 (600°C) (5 g/L)	NaCl (50 g/L)	3.9	92	This work
15	Mg/Al = 0.1 (5 g/L)	NaCl (50 g/L)	8.6	95	This work
16	Mg/Al = 0.2 (5 g/L)	NaCl (50 g/L)	8.6	95	This work
17	Mg/Al = 0.1 (3.3 g/L)	NaCl (50 g/L)	8.6	87	This work
18	Mg/Al = 0.1 (3.3 g/L) reuse	NaCl (50 g/L)	8.6	98	This work

The presence of salt (NaCl) in the synthetic effluent (runs 10, 11, 12 and 13, Table 5) has similar scavenging effect for HO° as for DMP substrate for the initial rate of TOC removal for direct ozonation (with a decrease by a factor 1.7) and slightly less for catalytic ozonation (with a decrease by a factor 1.4). But, the main difference with DMP substrate is that the decrease of initial reaction rate resulted in a dramatic increase of the level of TOC removal, the latter being above 90% after 300 min reaction. The extent of TOC removal achieved, implying decomposition of acetic acid, led to the conclusion that a somewhat different, and more complex mechanism, was operating in this case. By reference to literature data it was therefore suggested [13] that PAH were oxidized by reaction with chlorine or chlorine radicals, within in addition, *in-situ* generation of HO° and hydrogen peroxide in the reaction medium, able to degrade acetic acid via the transient formation of peracetid acid, a powerful oxidant able to degrade PAH. This suggests two pathways for HO° generation: one from the hydroxyls of the catalysts and one from the decomposition of PAH. The following reactions are suggested:

1- production of HO° by the catalyst:

$$\text{Catalyst-OH} + O_3 \longrightarrow \text{HO°} \text{ (fast)}$$

2- degradation of phenols into carboxylic acids

$$\text{Phenols} + \text{HO°} \text{ or } O_3 \longrightarrow \text{acetic acid} > \text{formic acid} >> \text{oxalic acid}$$

3- scavenging effect of HO° by Cl^-:

$$Cl^- + \text{HO°} \longrightarrow \text{HOCl}^{-\circ}$$
$$\text{HOCl}^{-\circ} + H^+ \longrightarrow \text{Cl°} + H_2O$$

4- reactions of Cl^- derivatives with PAH:

$$Cl^- + O_3 \longrightarrow O_2 + ClO^-$$
$$Cl^- + ClO^- + 2H^+ \longrightarrow Cl_2 + H_2O$$
$$\text{Pyrene} + Cl_2 \longrightarrow \text{dihydroxypyrene} + H_2O_2 \longrightarrow \text{Pyrene-dione} + \text{Chloropyrene} + \text{HO°}$$
$$CH_3COOH + H_2O_2 \longrightarrow CH_3COOOH + H_2O$$
$$CH_3COOOH + \text{PAH} \longrightarrow \text{degradation products of PAH (carboxylic acids)}$$

5- final degradation of carboxylic acids:

$$\text{Carboxylic acids (except } CH_3COOH) + HO^\circ \text{ or } Cl_2 \longrightarrow CO_2 + H_2O$$

We suggest that a faster production of HO° by the catalyst could predominate on the reaction rate of the scavenging by Cl^- and reach higher initial degradation rate for saline produced water as obtained in the present work for γ-Al_2O_3 doped with Mg (runs 15 to 18, Table 5) and presented below.

Catalytic ozonation of saline synthetic produced water

The catalytic properties γ-Al_2O_3 modified with different metal oxides were evaluated in the ozonation the synthetic produced water. As shown in the experimental section the main characteristics of this effluent are: pH = 3.3 – 4.3, COD = 668 mg O_2/L, TOC = 216 mg/L, RedOx potential = 350 mV, Cl^- = 30 g/L.

After preliminary investigations, we chose to probe the more basic materials, *ie*, Mg/γ-Al_2O_3 (Mg/Al = 0.2), Mg/Cu/Al_2O_3 (sg) (Cu/Mg/Al = 0.2/0.2/1) > Mg/Cu/γ-Al_2O_3 (Cu/Mg/Al = 0.2/0.2/1), Mg/γ-Al_2O_3 (Mg/Al = 0.1) and the materials featuring the highest oxidative character, *ie*, Mg/Cu/γ-Al_2O_3 (Cu/Mg/Al = 0.2/0.2/1) > Cu/γ-Al_2O_3 (Cu/Al = 0.2) (Fig. 6). All the materials have been activated at 600 °C. Commercial γ-Al_2O_3 calcined and uncalcined have been used for comparison. Note that all catalysts featured similar textural properties (Table 3): specific surface areas close to 200 m^2/g, mesopore volumes of 0.4-0.7 mL/g, mesopore diameters of 10 nm and C_{BET} = 100-120 characteristic of hydroxylated surfaces.

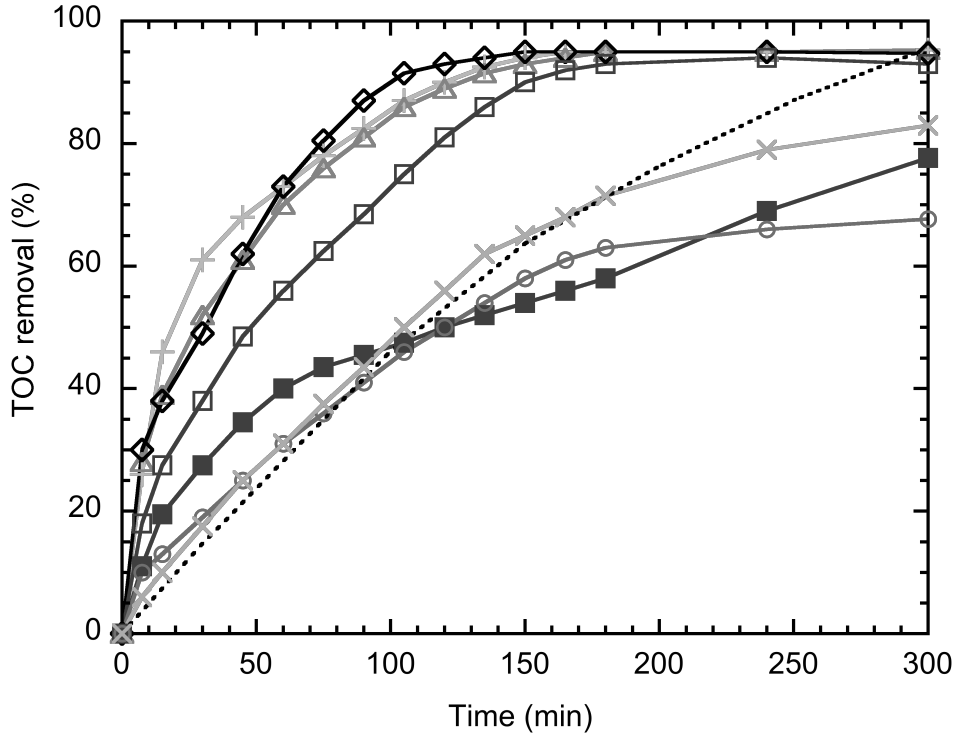

Fig. 6. TOC removal (%) of saline petroleum effluent (initial TOC = 216 mg/L) as a function of ozonation time for the catalysts (5 g/L): (■) uncalcined γ-Al_2O_3, (□) γ-Al_2O_3 calcined at 600 °C and materials calcined at 600 °C with (+) Mg/Cu/γ-Al_2O_3 (Mg/Cu/Al = 0.2/0.2/1), (Δ) Mg/γ-Al_2O_3 (Mg/Al = 0.1), (◊) Mg/γ-Al_2O_3 (Mg/Al = 0.2), (O) Cu/γ-Al_2O_3 (Cu/Al = 0.2), (X) Mg/CuO/Al_2O_3 (Mg/Cu/Al = 0.2/0.2/1) prepared by sol-gel (sg). Dashed line represents the ozonation without catalysts taken from ref. 13.

No increase of temperature was noticed during catalytic ozonation reactions. The pH of the effluent increased from pH = 3 – 4 to 5 - 7 when catalysts (freshly dried at 105°C) were added to the reaction mixture (Fig. S16). A brown color appeared as soon as ozone was introduced in the reactor and disappeared after 20 – 50 min (Fig. S17) when the RedOx potential jumped steeply from 350 to 1000 mV (Fig. S18). Similar brown color has already been reported during the oxidation of phenol with HO° radicals into ortho- and para-benzoquinone [39]. The transient color change is attributed to the formation of dihydroxylated ring intermediates, which can react with their own quinones to generate charge-transfer complexes, which take a dark color at low concentrations. Para-benzoquinone has been used as HO° radicals scavenger in the catalytic ozonation of AO7 ($C_{16}H_{11}N_2NaO_4S$) dye with Cu/Al_2O_3 catalyst [40]. Benzoquinone drastically inhibited the catalytic activity of Cu/Al_2O_3 due to rapid reaction with HO°. Therefore we may assume that in our case phenol is first oxidized through direct ozonation into benzoquinone, which then rapidly reacts with HO° to give oxidized products.

When all benzoquinone is transformed, the coloration disappears and the concentration of ozone in solution increases. During the first 20 to 50 min, the TOC values decreased but in a different way, depending on the catalyst: 20% of TOC removal for $CuO/\gamma\text{-}Al_2O_3$ (Cu/Al = 0.2), $Mg/Cu/Al_2O_3$ (sg) (Cu/Mg/Al = 0.2/0.2/1) and 30-50% of TOC removal for $\gamma\text{-}Al_2O_3$ calcined at 600 °C, $Mg/\gamma\text{-}Al_2O_3$ (Mg/Al = 0.1 and 0.2), $Mg/Cu/\gamma\text{-}Al_2O_3$ (Cu/Mg/Al = 0.2/0.2/1) (Fig. S18).

TOC removal level increased with ozonation time (Fig. 6) to reach 70-80% after 5 h for $Cu/\gamma\text{-}Al_2O_3$ (Cu/Al = 0.2), $Mg/Cu/Al_2O_3$ (sg) (Cu/Mg/Al = 0.2/0.2/1) and uncalcined $\gamma\text{-}Al_2O_3$. For $\gamma\text{-}Al_2O_3$ calcined at 600 °C and Mg based catalysts prepared by incipient wetness impregnation on $\gamma\text{-}Al_2O_3$ ($Mg/\gamma\text{-}Al_2O_3$, Mg/Al = 0.1 and 0.2, and $Mg/Cu/\gamma\text{-}Al_2O_3$, Cu/Mg/Al = 0.2/0.2/1), TOC removal reached 95% after 5 h (Fig. 6**,** runs 15, 16, Table 5**)**. The evolution of TOC with these materials reveals that the main TOC reduction occurs within the first 2 h (> 90%).

Uncalcined $\gamma\text{-}Al_2O_3$ was not active in catalytic ozonation, whereas $\gamma\text{-}Al_2O_3$ calcined at 600 °C was active. This observation could explain why some authors consider $\gamma\text{-}Al_2O_3$ as excellent in catalytic ozonation due to the generation of HO° [13,41,42], while some others found that $\gamma\text{-}Al_2O_3$ does not catalyze the removal of pollutants such as hydrocarbons [21,41,42]. $\gamma\text{-}Al_2O_3$ needs activation before to be used in catalytic ozonation. A good reproducibility of the results of literature was obtained with $\gamma\text{-}Al_2O_3$ calcined at 600 °C (runs 13 and 14, Table 5).

The catalyst with only oxidative character such as $Cu/\gamma\text{-}Al_2O_3$ (Cu/Al = 0.2) was poorly active in catalytic ozonation of the saline effluent as TOC removal was only around 65% after 5 h ozonation (Fig. 6) inferior to the TOC removal by single ozonation [13]. Cu leaching was also observed during catalytic ozonation as after reaction $Cu/\gamma\text{-}Al_2O_3$ revealed a ratio Cu/Al of 0.12 instead of 0.20. On the contrary, all catalysts featuring high basicity properties proved very active, except the catalyst prepared by sol-gel, $Mg/Cu/Al_2O_3$ (sg) (Cu/Mg/Al = 0.2/0.2/1). This catalyst was destroyed and densified during catalytic ozonation, its surface area has decreased from 300 to 20 m^2/g (Table 3), which explains its low activity.

Catalysts prepared by incipient wetness impregnation exhibited a slight decrease (~ 25%) of surface area and pore volume after ozonation (S = 150-190 m^2/g, V = 0.40-0.60 mL/g) (Table 3) with a preservation of their molar composition, except $Mg/Cu/\gamma\text{-}Al_2O_3$ (Cu/Mg/Al =

0.2/0.2/1). In this case a large amount of Cu was leached during catalytic ozonation leading to 0.003 < Cu/Al < 0.07 measured by EDS on the solid. Therefore, only the basic character of this catalyst accounted for its high catalytic activity. Mg/Cu/γ-Al_2O_3 (Cu/Mg/Al = 0.2/0.2/1) showed the same activity as Mg/γ-Al_2O_3 (Mg/Al = 0.2) (Fig. 6).

From the results above, it appears that surface basicity is the only requirement to generate active and stable catalysts for catalytic ozonation of saline petroleum effluents while oxidative character do not play a significant role.

Mg/γ-Al_2O_3 (Mg/Al = 0.1 and 0.2) catalysts prepared by incipient wetness impregnation showed higher activity than γ-Al_2O_3 calcined at 600 °C with a faster rate of pollutants degradation. After 1 h ozonation, levels of TOC removal were 55.5, 69.4 and 73.7% for γ-Al_2O_3, Mg/γ-Al_2O_3 (Mg/Al = 0.1 and 0.2), respectively. The initial reaction rate of Mg/γ-Al_2O_3 catalysts increased by 2.2 in comparison to γ-Al_2O_3 and by a factor 12 in comparison to direct ozonation (runs 11, 14, 15 to 18, Table 5). After 2 h reaction, the levels of TOC removal were 80.5, 90.3 and 93.9% and after 5 h they reached 92% for γ-Al_2O_3 and 95% for Mg/γ-Al_2O_3 (Mg/Al = 0.1 and 0.2) (Fig. 6).

Mg/γ-Al_2O_3 (Mg/Al = 0.1) exhibited similar but slightly lower catalytic activity in comparison to Mg/γ-Al_2O_3 (Mg/Al = 0.2), due to its slightly lower basicity, evidenced by a slightly lower pH increase during ozonation (Fig. S19). After 5 h of catalytic ozonation, the effluents featured pH values of 8.6 and 9.2 for Mg/γ-Al_2O_3 (Mg/Al = 0.1 and 0.2), respectively. However Mg/γ-Al_2O_3 (Mg/Al = 0.1) was the most efficient catalyst in terms of amounts of ozone consumed for the degradation of pollutants. It allowed less ozone consumption in comparison to all other catalyst with 12 g of consumed ozone per g of carbon mineralized (Fig. S20, S21) corresponding to 3 moles of O_3 per mole of C mineralized. This catalyst Mg/γ-Al_2O_3 (Mg/Al = 0.1) might be considered among the most efficient catalysts for catalytic ozonation of saline produced water.

Catalysts solely composed of MgO nanoparticles have already proven good catalysts for catalytic ozonation of quinolone by generating HO° radicals [43]. They have shown relatively good stability in reuse, but with a progressive decrease of activity after each reuse, leading to a decrease of degradation level of quinolone from 100 to 93% after 5 cycles. This loss of

activity was attributed to the increase of the size of the MgO NPs from 17 to 37 nm by sintering during ozonation, reducing its overall activity [43].

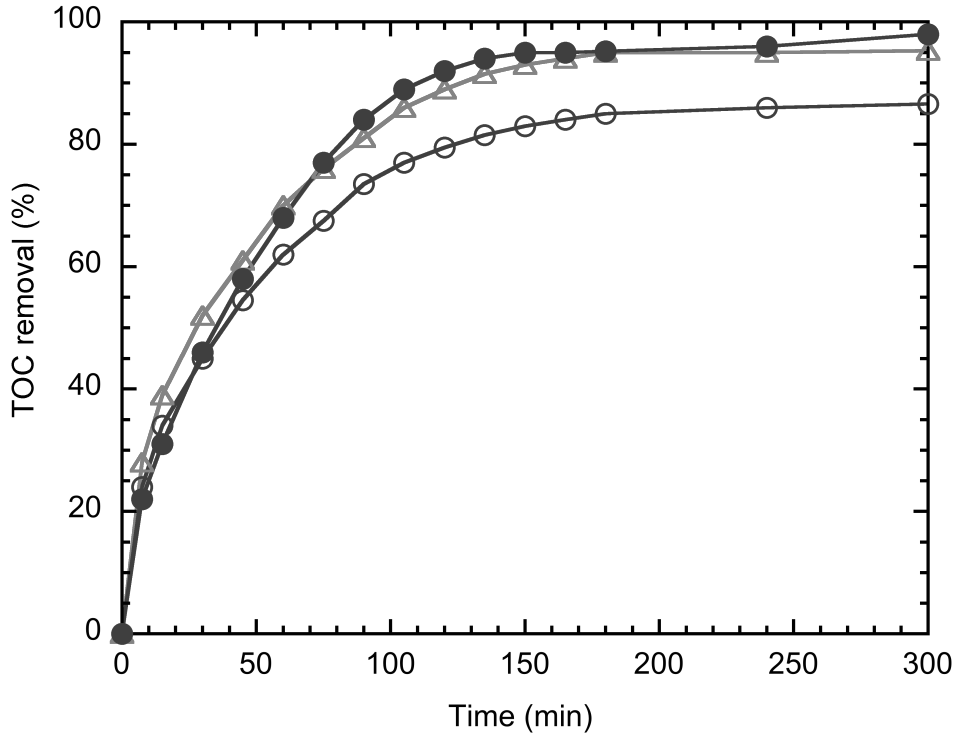

Fig. 7. TOC removal (%) of saline petroleum effluents (initial TOC = 216 mg/L) as a function of ozonation time for Mg/γ-Al_2O_3 (Mg/Al = 0.1) calcined at 600 °C with (O) 3.3 and (Δ) 5 g/L of catalyst and (●) in reuse with 3.3 g/L of catalyst.

The stability of Mg/γ-Al_2O_3 (Mg/Al = 0.1) catalyst was evaluated in a second run of ozonation (runs 17, 18, Table 5). The catalyst recovered by filtration after a first run has been washed with demineralized water and dried at 105 °C. 3.3 g of catalyst were thus recovered. During the second run, Mg/γ-Al_2O_3 (Mg/Al = 0.1) catalyst (3.3 g/L) exhibited an outstanding improvement of activity, which reached 98% TOC removal after 5 h reaction (Fig. 7). For a better comparison with the fresh catalyst Mg/γ-Al_2O_3 (Mg/Al = 0.1), an ozonation test with the same amount of fresh catalyst (3.3 g/L) was performed and revealed a much lower efficiency with 87 % TOC removal after 5 h. To understand the origin of the increase of efficiency of Mg/γ-Al_2O_3 (Mg/Al = 0.1) after an ozonation cycle, the textural and structural features of the used catalysts were examined by nitrogen adsorption, TGA, SEM (Fig. 8), XRD (Fig. 9) and TEM (Fig. 10-13).

Textural and structural characterization of the catalysts after ozonation

After 1 and 2 ozonation runs the catalyst Mg/γ-Al_2O_3 (Mg/Al = 0.1 and 0.2) preserved their textural properties: specific surface areas, mesopore volumes and mesopore diameters are similar (Table 3).

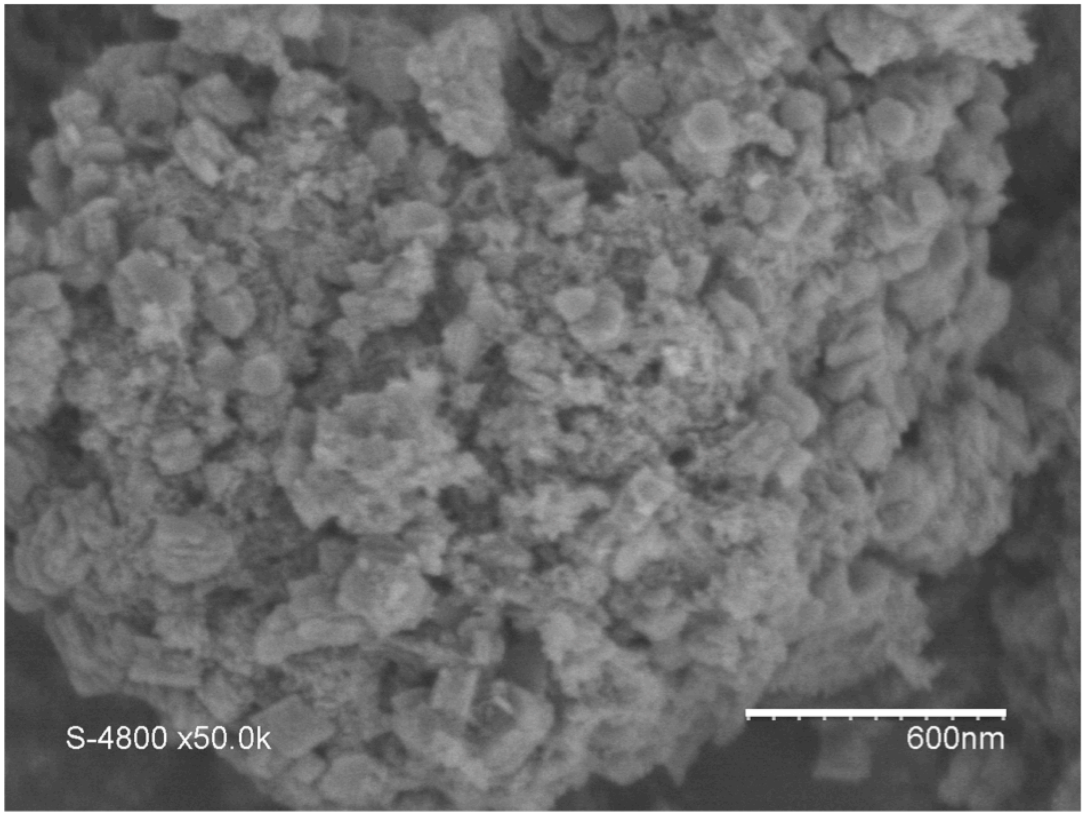

Fig. 8. SEM pictures of Mg/γ-Al_2O_3 (Mg/Al = 0.1) after two catalytic ozonations.

SEM pictures of γ-Al_2O_3 and Mg/γ-Al_2O_3 (Mg/Al = 0.1 and 0.2) after ozonation showed grains with a rough surface and the presence of some round nanoparticles at the surface of the grains, with a slightly larger amount of nanoparticles in the surface of Mg/γ-Al_2O_3 (Mg/Al = 0.2) (Fig. S22). After the second ozonation run, Mg/γ-Al_2O_3 (Mg/Al = 0.1) showed clearly the appearance of a large amount of round and square nanoparticles of 100 nm in size at the surface of the grains (Fig. 8). TEM pictures of γ-Al_2O_3 after ozonation revealed the classical morphology of needles-like structure of alumina with very few round nanoparticles (100 nm) at the surface (Fig. 9). TEM pictures of Mg/γ-Al_2O_3 (Mg/Al = 0.1) after one ozonation showed the classical morphology of γ-Al_2O_3 with, in addition, a large population of nanoparticles (100 nm) (Fig. 10). Some of the nanoparticles started to segregate from the grains surface. After the second ozonation run, the segregation of the nanoparticles from the surface increased and some separate discrete phase appeared, formed by an aggregation of nanoparticles (Fig. 11). TEM pictures of Mg/γ-Al_2O_3 (Mg/Al = 0.2) after one ozonation run

showed the typical morphology of γ-Al_2O_3, some nanoparticles (100 nm) at the surface of the grains, with, in addition, some large plates characteristic of a lamellar structure (Fig. 12).

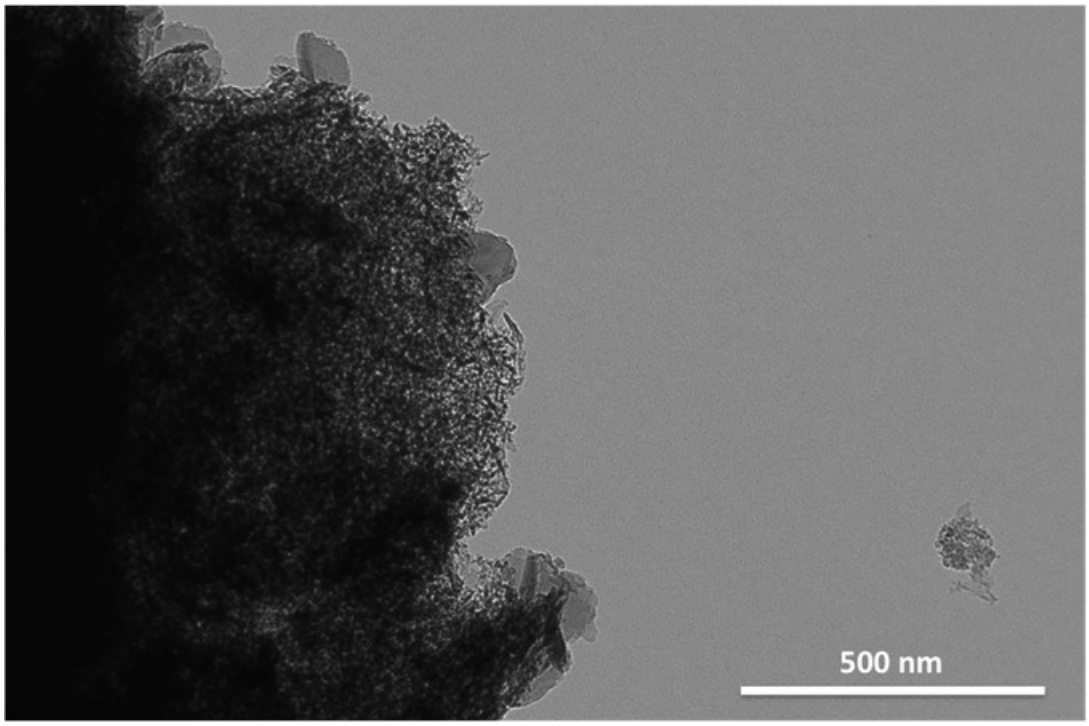

Fig. 9. TEM pictures of γ-Al_2O_3 (calcined 600 °C) after one catalytic ozonation.

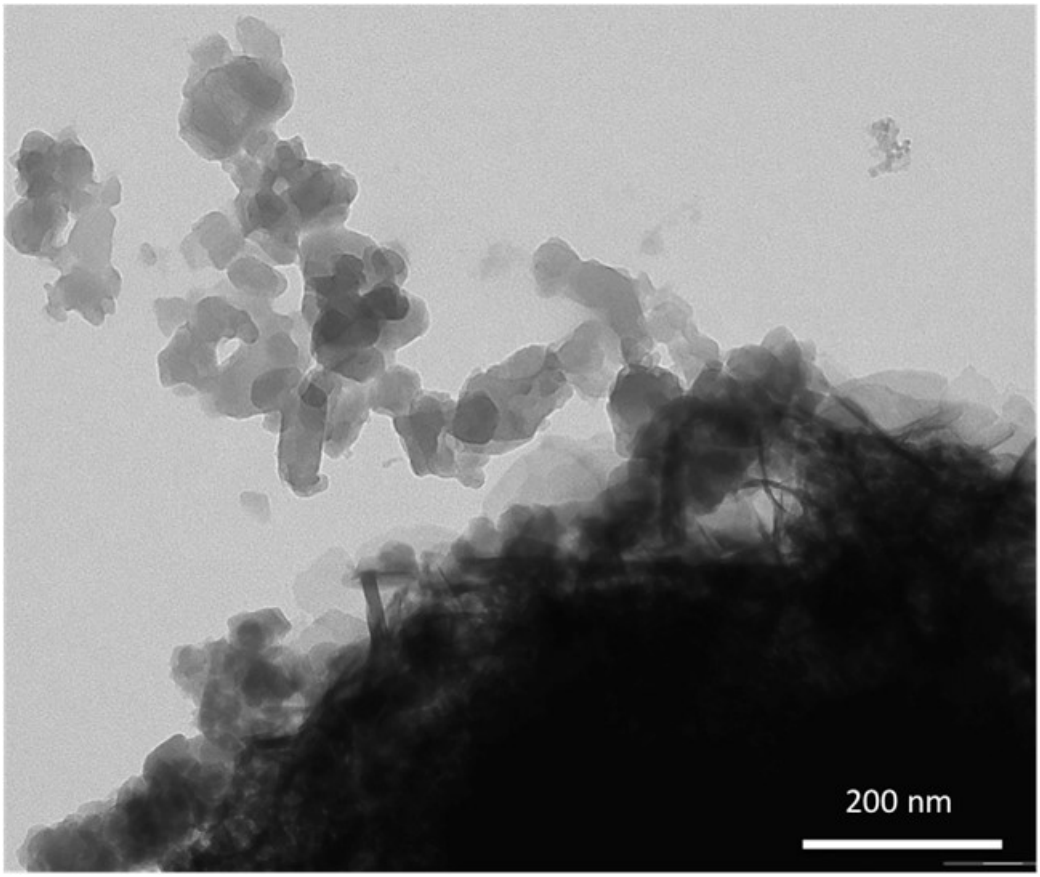

Fig. 10. TEM pictures of Mg/γ-Al_2O_3 (Mg/Al = 0.1) after one catalytic ozonation.

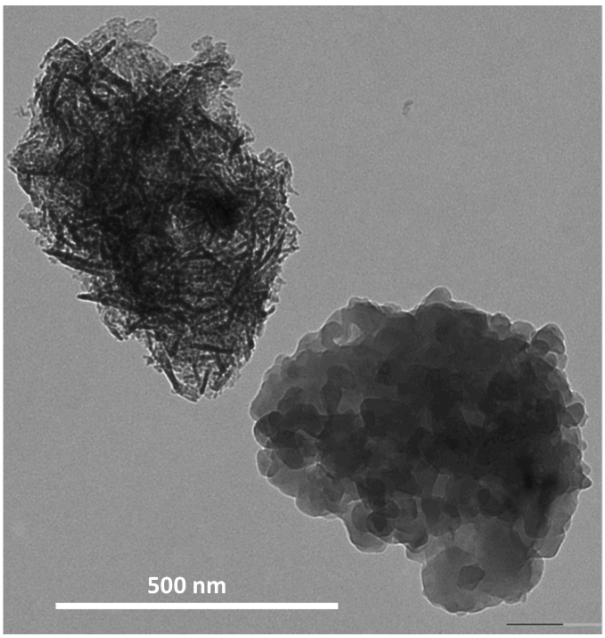

Fig. 11. TEM pictures of Mg/γ-Al_2O_3 (Mg/Al = 0.1) after two catalytic ozonations.

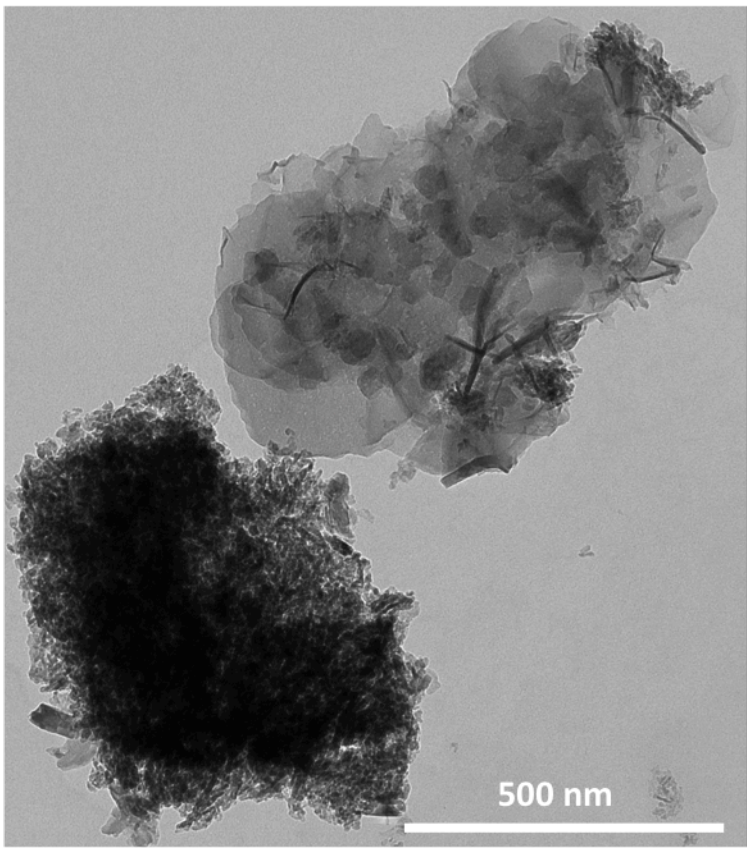

Fig. 12. TEM pictures of Mg/γ-Al_2O_3 (Mg/Al = 0.2) after one catalytic ozonation.

XRD patterns of Mg/γ-Al_2O_3 (Mg/Al = 0.1) after 1 and 2 ozonation experiments showed additional diffractions peaks apart from the alumina structure, attributed to an orthorhombic magnesium aluminium spinel $MgAl_2O_4$ phase [44], which increased in intensity after the second ozonation (Fig. 13). For Mg/γ-Al_2O_3 (Mg/Al = 0.2) after 1 ozonation run, XRD

showed a similar spectrum with peaks attributed to a spinel phase with a lower intensity than for Mg/γ-Al_2O_3 (Mg/Al = 0.1) and the apparition of a hydrotalcite-like phase (named, Layered Double Hydroxide (HDL)) of general formula $Mg_{1-x}Al_x(OH)_2,X_{x/n}^{n-}$, m H_2O ($0.2 < x < 0.4$, corresponding to $2 < Mg/Al < 4$, and $X = CO_3^{2-}$, Cl^-). The calculated interlayer distance of d_{003} = 0.78 nm (Fig. 13) indicates the presence of Cl^- as compensating anion due to the excess of NaCl. The formation of the LDH phase results from the rehydroxylation of the Mg/Al mixed-oxide present on the γ-Al_2O_3 surface at the high pH of the solution (pH = 9). The LDH phase is not detected by XRD for Mg/γ-Al_2O_3 (Mg/Al = 0.1) due to its too low amount or to the slightly lower pH (8.5) of the solution (Fig. S19).

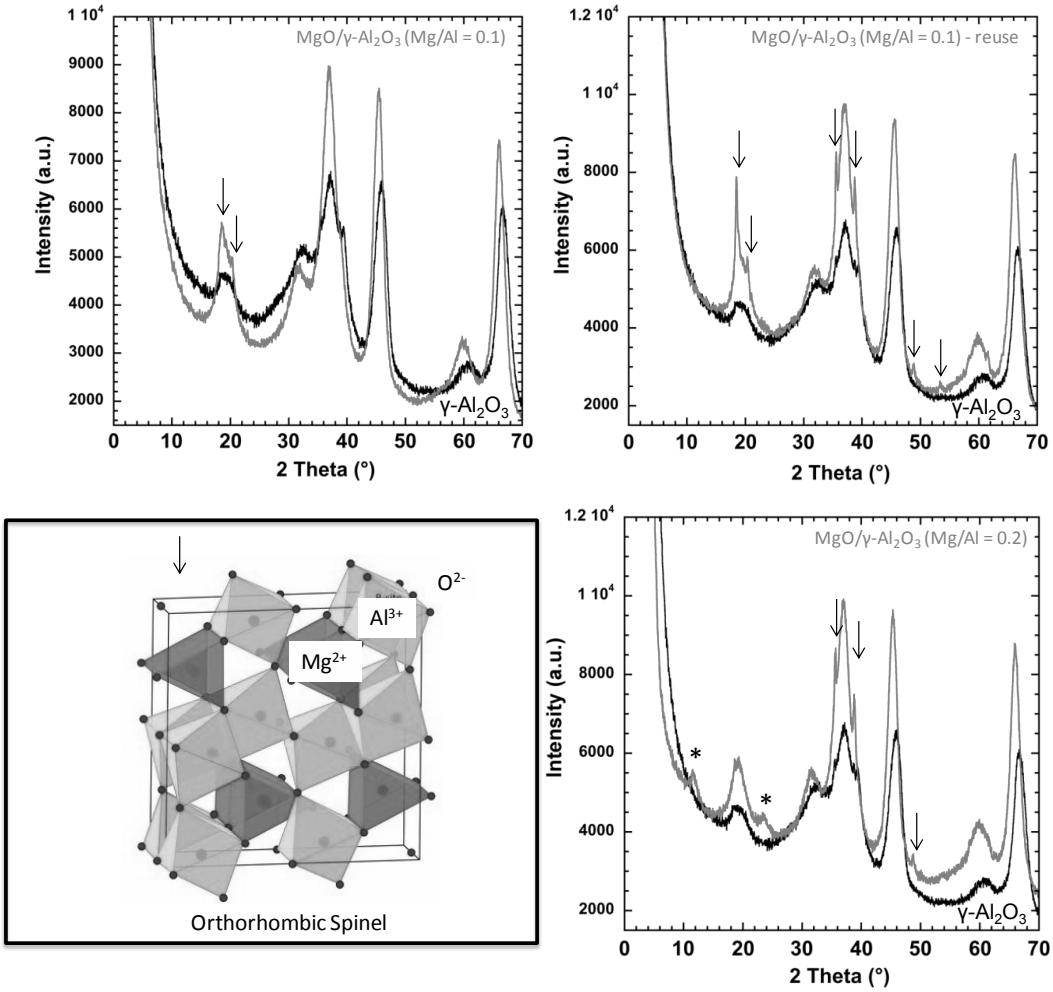

Fig. 13. XRD pattern of catalysts after catalytic ozonation: (grey) Mg/γ-Al_2O_3 (Mg/Al = 0.1) after 1 and 2 ozonation (reuse) and Mg/γ-Al_2O_3 (Mg/Al = 0.2) after 1 ozonation. For comparison in each graph (black) calcined γ-Al_2O_3 (600 °C) after 1 ozonation. Diffraction peak for orthorhombic spinel (arrows) and LDH - d_{100} = 0.78 nm (*). Schematic representation of the orthorhombic spinel structure.

The formation of orthorhombic spinel phase $MgAl_2O_4$ and possibly LDH phase are therefore responsible for the outstanding activity of the catalysts Mg/γ-Al_2O_3 (Mg/Al = 0.1) in catalytic ozonation of saline petroleum effluent. In general, the catalytic use of cubic spinel $MgAl_2O_4$ has received significant attention as an alternative to traditional alumina-supported catalysts because of its high thermal stability and strong basicity [45]. $MgAl_2O_4$ is an important ceramic material due to its attractive combination of physical, chemical, optical and magnetic properties. It is mainly obtained as dense structures featuring very low surface areas. Efforts have been paid to synthesize ultrafine or nanosized powders of $MgAl_2O_4$ [44]. Nano-sized $MgAl_2O_4$ powders have been produced at 1150 °C for 4 h [46] or in an ultrasonic oxygen atomizer followed by a combustion at 2000 °C [44]. Round nanoparticles (< 60 nm) have been obtained featuring surface areas of 30-80 m^2/g [44]. Spinel $MgAl_2O_4$ can be produced at lower temperature (700 °C) by chlorination, while in air a temperature above 930 °C was necessary [47].

Recently, mesoporous flake-like cubic spinel $MgAl_2O_4$ nanoparticles (10 nm) featuring high surface area of 264 m^2/g with a mesopore diameter of 6 nm have been produced by the sol-gel process using nitrate salts of Al and Mg in the presence of propylene oxide and a calcination of 700 °C [48]. This material should be worth evaluation in catalytic ozonation. Such a flake-like morphology with a high surface area of 169 m^2/g is similar to that of the confidential commercial catalysts used by Sun et al. [42] for ozonation of non saline petroleum effluents, and could be therefore a spinel $CuAl_2O_4$. To the best of our knowledge, no spinel $MgAl_2O_4$ catalysts have been used in catalytic ozonation. Only $CuAl_2O_4$ and $Cu_xMg_{(1-x)}Al_2O_4$ (20 m^2/g) spinels have been reported, with the limitation of Cu leaching [31]. Authors showed slightly higher activity and stability for CuMgAl spinels in comparison to HDLs based materials (MgAl, MgFeAl and MgCuAl) [31].

In our study, spinel $MgAl_2O_4$ nanoparticles (100 nm) are produced at the surface of γ-Al_2O_3 under strong oxidizing conditions at ambient temperature from Mg/γ-Al_2O_3 (Mg/Al = 0.1) materials previously calcined at 600 °C. In recent literature, Mg/γ-Al_2O_3 (Mg/Al = 0.0025) was prepared by incipient wetness impregnation followed by a calcination at 550 °C and used in the catalytic ozonation (with a catalyst amount of 5 g/L) of non saline petroleum effluents featuring a pH of 8.15 containing 27% of organic alcohol and 25% of heterocyclic compounds [49]. Slightly higher efficiencies were found for Mg-Ce/γ-Al_2O_3 compared to Mg/γ-Al_2O_3, both featuring highest efficiencies than γ-Al_2O_3. After 40 min reaction, COD

removal was 34, 46 and 52% for γ-Al_2O_3, Mg/γ-Al_2O_3 and Mg-Ce/γ-Al_2O_3, respectively. Increasing the Mg amount (Mg/Al = 0.0077) did not change the efficiency. Authors have shown that Mg deposited on γ-Al_2O_3 enhanced further HO° generation and that direct ozonation operated as well. The active catalytic surface promote formation of HO° from ozone, accelerating chemical degradation. Authors state that the density of surface OH groups stand in the order: γ-Al_2O_3 > Mg/γ-Al_2O_3 > Mg-Ce/γ-Al_2O_3 [49], suggesting that the strength of the basic sites was more important than the number of OH groups in determining catalytic efficiency. Interestingly, it was shown that Mg^{2+} was well dispersed on the γ-Al_2O_3 surface with strong interactions between Mg and γ-Al_2O_3 support and that the surface content of MgO was greater than that of the bulk [49].

In our case, TGA profiles and surface areas of γ-Al_2O_3 and Mg/γ-Al_2O_3 (Mg/Al = 0.1 and 0.2) are identical, revealing a same level of dehydroxylation, so a similar amount of surface –OHs (**Fig. S23**). However a slightly lower dehydroxylation degree was noticed for the Mg/γ-Al_2O_3 (Mg/Al = 0.1) after the second ozonation run, suggesting less surface OHs, whereas the ozonation efficiency was improved. A segregation of Mg at the surface of the alumina particles for MgO/γ-Al_2O_3 (Mg/Al = 0.1 and 0.2) could be at the origin of the activity enhancement through the formation of Mg rich phases as spinel and LDH at the surface. This segregation might be favored under strong oxidizing reaction conditions as ozonation since the spinel amount increased upon successive ozonation.

The promotional effect of surface spinels on the catalytic ozonation activity has been reported several times and attributed to the generation of oxygen vacancies. Two hypothesis have been put forward to account for this observation: either (i) a higher amount of active-OH groups on the surface by water adsorption producing more HO° radicals [50, 51] or (ii) reaction of ozone with vacancies producing very active superoxide radicals, which can in turn lead to formation of HO° radicals as well [52, 53]. In both cases the flow of radicals is increased. In TGA profiles (Fig. S23) the weight loss occurring between 150 and 200 °C could be attributed to some water molecules trapped into the spinel structure, supporting the first hypothesis.

The proposed mechanisms operate most probably for phenols and PAHs oxidation, but presumably not for other types of pollutants such as chlorinated compounds, which are not interacting with HO° but rather degraded by direct ozonation of adsorbed ozone with

adsorbed pollutants at the surface of the catalyst. In that case the process requires hydrophobic catalysts such as ZSM-5 zeolites with high Si/Al ratio [41]. A mixture of Mg/γ-Al_2O_3 (Mg/Al = 0.1) catalyst with silicalite-1 could represent a versatile catalyst for catalytic ozonation.

CONCLUSION

Previously, we have demonstrated that γ-Al_2O_3 was an efficient catalyst for ozonation as it produces HO° radicals from the reaction of O_3 with Al-OH basic sites. In the case of saline effluents, chloride ions play usually a very strong scavenging effect on HO° radicals, which increases with the amount of NaCl and account for 70% of HO° neutralization for NaCl = 50 g/L. However, when the effluents contained polycyclic aromatic hydrocarbons (PAHs) the opposite effect was observed. It was proposed that PAHs react with Cl° or Cl_2, coming from reaction of Cl^- with HO° and Cl^- with O_3, respectively, to produce new HO° and H_2O_2, which are able to degrade carboxylates into CO_2 and HO^- leading to an increase of pH. In the case of petroleum saline (NaCl 50 g/L) effluents containing acetic acid (30%), phenols and PAHs, the combination of O_3, NaCl and PAHs allow a mineralization of 90% of the pollutants in 5 h including the mineralization of acetic acid, which is the most resistant carboxylic acid to oxidize. The addition of γ-Al_2O_3 increases the rate of mineralization in comparison to O_3 with the same level of final mineralization.

In this study, in order to further improve catalytic ozonation, mesoporous alumina-based materials containing different promoters (Mg, Ca, Zn, Fe, Ba, Zr, Cu, Co, Ni, Ce, Ti) have been prepared either by incipient wetness on γ-Al_2O_3 particles or by direct sol-gel (sg) precipitation. These metals have been chosen to improve either the basicity and/or the oxidative character of alumina. A basicity scale in water has been developed based on the amount of benzoic acid adsorbed and the pH of the resulting solutions. An oxidative test has been developed based on the oxidation of benzyl alcohol into benzaldehyde in cyclohexane at 150 °C. The more basic solids were Mg-based materials with molar ratios: Mg/Al (0.2/1), Cu/Mg/Al (0.2/0.2/1)(sg) > Cu/Mg/Al (0.2/0.2/1), Mg/Al (0.1/1). The materials featuring the higher oxidative properties were CuO nanoparticles-based materials with Cu/Mg/Al (0.2/0.2/1) > Cu/Al (0.2/1), Cu/Mg/Al (0.1/0.1/1). All materials present high surface area, mesopore volumes and mesopore diameters similar to γ-Al_2O_3 (200 m^2/g, 0.6 mL/g, 11 nm diameter).

These materials were tested in the catalytic ozonation of a synthetic petroleum saline effluent representative of a produced water containing phenols, acetic acid and PAHs. The results show that: (1) γ-Al_2O_3 leads to an improvement of ozonation rate only if it is calcined at 600°C, (2) materials with only oxidative properties as Cu/Al (0.2/1) are not efficient, (3) basic materials are the most efficient. The rate of ozonation increases with the increase of basicity of the material, so with the Mg content. After 5 h ozonation, the pH of the solution initially at 3.3-4.3 has increased to 8.5 for Mg/Al (0.1/1) and to 9.2 for Mg/Al (0.2/1). Ozonation efficiency is only related to the basicity of the materials.

Materials prepared by incipient wetness on γ-Al_2O_3 particles maintain their textural characteristics (mesopore volume, diameter and surface area), whereas sol-gel materials are destroyed during ozonation. Mg/Al (0.2/1), Cu/Mg/Al (0.2/0.2/1), Mg/Al (0.1/1) catalysts lead to the highest rate of ozonation with a mineralization level > 90% after 2 h and 95% after 5 h. Ozonation leads to the leaching of copper in Cu/Mg based materials, whereas the composition of Mg/Al materials remains constant. Mg is the only efficient metal.

Mg/γ-Al_2O_3 (Mg/Al = 0.1) is the most efficient catalyst in terms of mineralization level and consumption of O_3 to oxidize the pollutants. Furthermore, this catalyst in reuse shows a remarkable improvement of catalytic activity with the highest level of mineralization (98%). This increase of catalytic ozonation activity in reuse has never been observed before and is attributed to the formation of nanoparticles of orthorhombic spinel structure ($MgAl_2O_4$) at the surface of the grains of γ-Al_2O_3 generating probably more HO° radicals. A catalyst formed only by nanoparticles of orthorhombic spinel structure $MgAl_2O_4$ could be an outstanding catalyst for ozonation. For the catalyst with higher Mg content Mg/γ-Al_2O_3 (Mg/Al = 0.2), some layered double hydroxide (LDH) are formed at the expense of the spinel. Both Mg/γ-Al_2O_3 oxides (Mg/Al = 0.1 and 0.2) catalysts are promising catalysts for ozonation of real saline petroleum effluents containing PAHs, such as produced water.

Acknowledgments

This research was funded by the TOTAL SA through a grant from Fondation Franco-Chinoise pour la Sciences et ses Applications (FFCSA). Authors thank Anne-Sophie Caen and Patrick Van Effenterre from FFCSA for their support. Authors thank Didier Tichit and Dan Lerner for fruitful discussions. The authors wish to acknowledge the support from the Chemistry Plateform of Campus in Montpellier (Plateform MEA University Montpellier), on which SEM, TEM and EDS experiments have been performed.

References

1 S. P. Ghuge, A. K. Saroha, J. Env. Manag. **211**, 83-102 (2018).
2 J. Nawrocki, B. Kasprzyk-Horden, Appl. Catal., A **99**, 27-42 (2010).
3 Y.M. Dong, K. He, B. Zhao, Y. Yin, L. Yin, A. Zhang, Catal. Commun. **8**, 1599-1603 (2007).
4 K. He, Y. M. Dong, Z. Li, L. Yin, A. M. Zhang, Y.C. Zhang, J. Hazard Mater. **159**, 587-592 (2008).
5 L. Huan, J. Shen, Z. Chen, Y. Liu, Appl. Catal., B **117**, 414-419 (2012).
6 D. S. Pines, D. A. Reckow, Ozone: Sci. Eng. **25**, 25-39 (2003).
7 J. M. Roscoe, J. P. D. Abbatt, J. Phys. Chem. A **109**, 9028-9034 (2005).
8 T. Zhang, C. Li, J. Ma, H. Tian, Z. Qiang, Appl. Catal., B **82**, 131-137 (2008).
9 T. Zhang, J. Lu, J. Ma, Z. Qiang, Chemosphere 71, 911- 921 (2008).
10 Y. Yang, J. Ma, Q. Qin, X. Zhai, J. Mol. Cat. A: Chem. **267**, 41-48 (2007).
11 P. C. C. Faria, J. J. M. Orfao, M. F. M. Pereira, Appl. Catal., B **79**, 237-243 (2008).
12 M. Sanchez-Polo, J. Rivera-Utilaa, Carbon **41**, 303-307 (2003).
13 J. Vittenet, W. Aboussaoud, J. Mendret, J-S. Pic, H. Debellefontaine, N. Lesage, K. Faucher, M-H. Manero, F. Thibault-Starzyk, H. Leclerc, A. Galarneau, S. Brossillon, Appl. Catal., A **504**, 519-532 (2015).
14 F. Qi, B. Xu, Z. Chen, L. Zhang, D. Sun, Chem. Eng. J. **219**, 527-536 (2013).
15 A. Ikhlaq, D. R. Brown, B. Kasprzyk-Horden, Appl. Catal., B **129**, 437-449 (2013).
16 M. Ernst, F. Lutor, J-C. Schrotter, Appl. Catal., B **47**, 15-25 (2004).
17 F. Qi, Z. Chen, B. Xu, J. Shen, J. Ma, C. Joli, A. Heitz, Appl. Catal., B **84**, 684-690 (2008).
18 B. Kasprzyk-Horden, U. Raczyk-Stanislawiak, J. Swiertlik, J. Nawrocki, Appl. Catal., B **62**, 345-358 (2006).
19 J. Lin, A. Kawai, T. Nakajima, Appl. Catal., B **39**, 157-165 (2002).
20 F. Qi, Z. Chen, B. Xu, J. Ma, D. Sun, L. Zhang, Sep. Purif. Technol. **33**, 405-410 (2009).
21 S. T. Oyama, Catal. Rev. Sci. Eng. **42**, 279-322 (2000).
22 P. M. Alvarez, F. J. Beltran, J. P. Pocosatles, F. J. Masa, Appl. Catal., B **72**, 322-330 (2007).
23 B. Kasprzyk, J. Nawrocki, Ozone, Sci. Eng. **24**, 63-68 (2003).
24 B. Kasprzyk-Horden, P. Andrzejewski, A. Dabrowska, K. Czaczyk, J. Nawrocki, Appl. Catal., B **51**, 51-66 (2004).
25 S. Hartmann, A. Sachse, A. Galarneau, Materials **5**, 336-349 (2012).
26 J. Rodier, L'analyse de l'eau, eaux naturelles, eaux résiduelles, eaux de mer, 8eme Ed. Dunod, Paris, 1996, 527-529.
27 T. Garoma, M. D. Gurol, O. Osibodu, L. Thotakura, Chemosphere **73**, 825-831(2008).
28 A. Galarneau, D. Desplantier, R. Dutartre, F. di Renzo, Microporous Mesoporous Mater. **28**, 437-446 (1999).
29 R. Poreddy, C. Engelbrekt, A. Riisager, Catal. Sci. Tech. **5**, 2467-2477 (2015).
30 M. Salavati-Niasari, F. Davar, M. Farhadi, J. Sol-Gel Sci. Technol. **51**, 48-52 (2009).
31 S. S. Sable, F. Medina, S. Contreras, App. Catal., B **150-151**, 30-36 (2014).
32 J. Cai, S. Bennici, J. Shen, A. Auroux, Microporous Mesoporous Mater. **212**, 156-168 (2015).
33 H-S. Roh, I-H. Eum, D-W. Jeong, B. E. Yi, J-G. Na, C. H. Ko, Catal. Today **164**, 457-460 (2011).
34 E. Trejo, M. S. Rana, J. Ancheyta, Catal. Today **130**, 327-336 (2008).

35 I. Vazquez-Garrido, A. Lopez-Benitez, G. Berhault, A. Guevara-Lara, Fuel **236**, 55-64 (2019).
36 Y. Wang, Y. H. Chin, R. T. Rozmiarek, B. R. Johnson, Y. Gao, J. Watson, A. Y. L. Tonkovich, D. P. Vander Wiel, Catal. Today **98**, 575-581(2004).
37 R. J. H. Grisel, B. E. Nieuwenhuys, J. Catal. **199**, 48-59 (2001).
38 J. Vittenet, J. Rodriguez, E. Petit, D. Cot, J. Mendret, A. Galarneau, S. Brosillon, , Microporous Mesoporous Mater., **189**, 200-209 (2014).
39 F. Mijangos, F. Varona, N. Villota, Environ. Sci. Technol. **40**, 5538 -5543 (2006).
40 Y. Xu, Z. Lin, Y. Zheng, J-P. Dacquin, S. Royer, H. Zhang, Sci. Total Environ. **651**, 2585-2596 (2019).
41 A. Ikhlaq, B. Kasprzyk-Horden, App. Catal., B **200**, 274 – 282 (2017).
42 X. Sun, C. Wu, Y. Zhou, W. Han, Chem. Eng. J. **369**, 100-108 (2019).
43 H. Zhu, W. Ma, H. Han, Y. Han, W. Ma, Chem. Eng. J. **327**, 91-99 (2017).
44 T. R. Hinklin, R. M. Laine, Chem. Mater. **20**, 553-558 (2008).
45 J. Salmones, J. A. Galicia, J. A. Wang, M. A. Valenzuela, G. Aguilar-Rios, J. Mater. Sci. Lett. **19**, 1033 (2000).
46 J. Zhang, T. Lu, X. Chang, N. Wei, W. Xu, J. Phys. D: Appl. Phys. **42**, 052002 (2009).
47 P. Orosco, L. Barbosa, M. del Carmen Ruiz, Mater. Res. Bull. **59**, 337 – 340 (2014).
48 N. Habibi, Y. Wang, H. Arandiyan, M. Rezaei, Adv. Powder Tech. **28**, 1249-1257 (2017).
49 C. Chen, Y. Chen, B. A. Yosa, Y. Du, Y. Wang, Q. X. Li, L. Yi, S. Guo, Q. Wang, Catalysts, **7**, 72-87 (2017).
50 W. Zhao, Q. Zhong, J. Ding, Z. Deng, L. Guo, F. Song, R.S.C. Adv. **6**, 115213-115221 (2016).
51 L. F. Liotta, M. Ousmane, G. D. Carlo, G. Pantaleo, G. Deganello, G. Marc, L. Retailleau, A. Giroir-Fendler, Appl. Catal., A **347**, 81–88 (2008).
52 J. Li, H. Na, X. Zeng, T. Zhu, Z. Liu, Appl. Surf. Sci. **311**, 690–696 (2014).
53 M. Jin, J. W. Kim, J. M. Kim, J. Jurng, G.-N. Bae, J.-K. Jeon, Y.-K. Park, Powder Technol. **214**, 458–462 (2011).